

AD-A280 987



①

# Semiannual Technical Report

## Atomic Layer Epitaxy of Group IV Materials: Surface Processes, Thin Films, Devices and Their Characterization

DTIC  
ELECTE  
JUL 0 1994  
S B D

Supported under Grant #N00014-91-J-1416  
Office of the Chief of Naval Research  
Report for the period 1/1/94-6/30/94

DTIC QUALITY INSPECTED 8

R. F. Davis, S. Bedair\*, N. A. El-Masry and J. T. Glass  
K. S. Ailey, P. Goeller, S. King, J. Sumakeris,  
D. Tucker and L. Tye  
c/o Materials Science and Engineering Department  
and \*Electrical and Computer Engineering Department  
North Carolina State University  
Campus Box 7907  
Raleigh, NC 27695-7907

DISTRIBUTION STATEMENT A  
Approved for public release  
Distribution Unlimited

4596 94-20012



June, 1994

94 6 29 079

**REPORT DOCUMENTATION PAGE**

Form Approved  
OMB No. 0704-0188

Public reporting burden for this collection of information is estimated to average 1 hour per response, including the time for reviewing instructions, searching existing data sources, gathering and maintaining the data needed, and completing and reviewing the collection of information. Send comments regarding this burden estimate or any other aspect of this collection of information, including suggestions for reducing this burden to Washington Headquarters Services, Directorate for Information Operations and Reports, 1215 Jefferson Davis Highway, Suite 1204, Arlington, VA 22202-4302, and to the Office of Management and Budget Paperwork Reduction Project (0704-0188), Washington, DC 20503.

1. AGENCY USE ONLY (Leave blank)	2. REPORT DATE June, 1994	3. REPORT TYPE AND DATES COVERED Semiannual Technical 1/1/94-6/30/94
----------------------------------	------------------------------	---

4. TITLE AND SUBTITLE Pseudo-morphic Semiconducting Heterostructures from Combinations of AlN, GaN and Selected SiC Polytypes: Theoretical Advancement and its Coordination with Experimental Studies of Nucleation, Growth, Characterization and Device Development	5. FUNDING NUMBERS 414s007---01 1114SS N00179 N66005 4B855
6. AUTHOR(S) Robert F. Davis	

7. PERFORMING ORGANIZATION NAME(S) AND ADDRESS(ES) North Carolina State University Hillsborough Street Raleigh, NC 27695	8. PERFORMING ORGANIZATION REPORT NUMBER N00014-90-J-1427
---	--

9. SPONSORING/MONITORING AGENCY NAME(S) AND ADDRESS(ES) Sponsoring: ONR, Code 314, 800 N. Quincy, Arlington, VA 22217-5660 Monitoring: Office of Naval Research Resider The Ohio State University Research Center 1960 Kenny Road Columbus, OH 43210-1063	10. SPONSORING/MONITORING AGENCY REPORT NUMBER
--	--

11. SUPPLEMENTARY NOTES

12a. DISTRIBUTION/AVAILABILITY STATEMENT Approved for Public Release; Distribution Unlimited	12b. DISTRIBUTION CODE
---	------------------------

13. ABSTRACT (Maximum 200 words)

The viability of Si<sub>2</sub>Cl<sub>6</sub>, C<sub>2</sub>H<sub>2</sub> and C<sub>2</sub>H<sub>4</sub> as precursors for chemically self-limiting ALE of SiC has been investigated via XPS and LEED. Si<sub>2</sub>Cl<sub>6</sub> readily adsorbs in a self-limiting manner on a Si(100) surface; however, neither hydrocarbon will adsorb or react with a Cl-terminated Si surface to 475°C. Conversely, partial chlorination of Si(100) saturated with C<sub>2</sub>H<sub>2</sub> and C<sub>2</sub>H<sub>4</sub> does occur and implies that Si<sub>2</sub>Cl<sub>6</sub> will adsorb/react with a hydrocarbon terminated surface. Layer-by-layer growth of β-SiC on Si(100) or 6H-SiC has been achieved with a carrier concentration of ≈10<sup>17</sup> cm<sup>-3</sup>. P-type doping with Al has allowed the achievement of hole concentrations of 4×10<sup>18</sup> - 2 10<sup>20</sup> cm<sup>-3</sup>. Efforts to produce an HBT using β-SiC emitters is described. Ni<sub>3</sub>Si has been employed for the deposition of diamond because of the close lattice match. Under the same growth conditions, diamond particles were obtained on the Ni<sub>3</sub>Si, but only diamond-like C and graphite on pure Ni substrates. Evidence of oriented particles was observed. REED and TEM of cerium oxide films grown on Si(111) substrates has revealed the formation of a dual amorphous layer of CeO<sub>x</sub> and SiO<sub>2</sub> at the Si interface followed by a layer of CeO<sub>2</sub>. Post annealing in dry oxygen caused the CeO<sub>x</sub> layer to disappear and the SiO<sub>2</sub> layer to thicken. D<sub>it</sub> = 6×10<sup>11</sup> cm<sup>-2</sup> and Q<sub>f</sub> = 5×10<sup>11</sup> cm<sup>-2</sup>. The structure exhibits a high capacitance due to the large dielectric constant of CeO<sub>2</sub> and has electrical properties comparable with those of other reported gate insulators on Si.

14. SUBJECT TERMS atomic layer epitaxy (ALE), silicon carbide (SiC), diamond, CeO <sub>2</sub> , C <sub>2</sub> H <sub>2</sub> , C <sub>2</sub> H <sub>4</sub> , Si <sub>2</sub> Cl <sub>6</sub> , Ni <sub>3</sub> Si, layer-by-layer growth, electrical properties, heterojunction bipolar transistor (HBT)	15. NUMBER OF PAGES 42
16. PRICE CODE	

17. SECURITY CLASSIFICATION OF REPORT UNCLAS	18. SECURITY CLASSIFICATION OF THIS PAGE UNCLAS	19. SECURITY CLASSIFICATION OF ABSTRACT UNCLAS	20. LIMITATION OF ABSTRACT SAR
---	--	---	-----------------------------------

## Table of Contents

I. Introduction	1
II. Routes to Chemically Self-Limiting ALE of SiC	4
III. Layer-by-Layer Deposition of SiC Thin Films: Growth, Characterization and Device Development	12
IV. Growth of Diamond Particles on a Ni <sub>3</sub> Si Substrate	29
V. Electrical Characterization of Epitaxial CeO <sub>2</sub> on Si (111)	35
VI. Distribution List	42

<b>Accession For</b>	
NTIS GRA&I	<input checked="" type="checkbox"/>
DTIC TAB	<input type="checkbox"/>
Unannounced	<input type="checkbox"/>
Justification	
By	
Distribution/	
Availability Codes	
Dist	Avail and/or Special
A-1	

## I. Introduction

Atomic layer epitaxy (ALE) is the sequential chemisorption of one or more elemental species or complexes within a time period or chemical environment in which only one monolayer of each species is chemisorbed on the surface of the growing film in each period of the sequence. The excess of a given reactant which is in the gas phase or only physisorbed is purged from the substrate surface region before this surface is exposed to a subsequent reactant. This latter reactant chemisorbs and undergoes reaction with the first reactant on the substrate surface resulting in the formation of a solid film. There are essentially two types of ALE which, for convenience, shall be called Type I and Type II.

In its early development in Finland, the Type I growth scenario frequently involved the deposition of more than one monolayer of the given species. However, at that time, ALE was considered possible only in those materials wherein the bond energies between like metal species and like nonmetal species were each less than that of the metal-nonmetal combination. Thus, even if multiple monolayers of a given element were produced, the material in excess of one monolayer could be sublimed by increasing the temperature and/or waiting for a sufficient period of time under vacuum. Under these chemical constraints, materials such as GaAs were initially thought to be improbable since the Ga-Ga bond strength exceeds that of the GaAs bond strength. However, the self-limiting layer-by-layer deposition of this material proved to be an early example of Type II ALE wherein the trimethylgallium (TMG) chemisorbed to the growing surface and effectively prevented additional adsorption of the incoming metalorganic molecules. The introduction of As, however caused an exchange with the chemisorbed TMG such that a gaseous side product was removed from the growing surface. Two alternating molecular species are also frequently used such that chemisorption of each species occurs sequentially and is accompanied by extraction, abstraction and exchange reactions to produce self-limiting layer-by-layer growth of an element, solid solution or a compound.

The Type II approach has been used primarily for growth of II-VI compounds [1-13]; however, recent studies have shown that it is also applicable for oxides [14-18], nitrides [19], III-V GaAs-based semiconductors [20-33] and silicon [34-36]. The advantages of ALE include monolayer thickness control, growth of abrupt interfaces, growth of uniform and graded solid solutions with controlled composition, reduction in macroscopic defects and uniform coverage over large areas. A commercial application which makes use of the last attribute is large area electroluminescent displays produced from II-VI materials. Two comprehensive reviews [37,6], one limited overview [38] and a book [39] devoted entirely to the subject of ALE have recently been published.

The materials of concern in this program include silicon carbide (SiC), diamond (C) and cerium dioxide (CeO<sub>2</sub>). Deposition of all three materials has been achieved using the progressive decomposition of metal-organic precursors (SiC and diamond) and laser ablation

(CeO<sub>2</sub>). In this reporting period, investigations concerned with (1) the viability of Si<sub>2</sub>Cl<sub>6</sub>, C<sub>2</sub>H<sub>2</sub> and C<sub>2</sub>H<sub>4</sub> as precursors for chemically self-limiting ALE of SiC, (2) the layer-by-layer growth of β-SiC on Si(100) or 6H-SiC and its n- and p-type doping, (3) the fabrication of an HBT using β-SiC emitters, (4) the application of Ni<sub>3</sub>Si as a substrate for the deposition of diamond and (5) the deposition and annealing of CeO<sub>x</sub>-based layers have been conducted.

The following sections introduce each topic, detail the experimental approaches, report the results to date and provide a discussion and a conclusion for each material. Each major section is self-contained with its own figures, tables and references.

#### References

1. T. Suntola and J. Antson, U.S. Patent 4,058,430 (1977).
2. M. Ahonen, M. Pessa and T. Suntola, *Thin Solid Films* **65**, 301 (1980).
3. M. Pessa, R. Makela, and T. Suntola, *Appl. Phys. Lett.* **38**, 131 (1981).
4. T. Yao and T. Takeda, *Appl. Phys. Lett.* **48**, 160 (1986).
5. T. Yao, T. Takeda, and T. Watanuki, *Appl. Phys. Lett.* **48**, 1615 (1986).
6. T. Yao, *Jpn. J. Appl. Phys.* **25**, L544 (1986).
7. T. Yao and T. Takeda, *J. Cryst. Growth* **81**, 43 (1987).
8. M. Pessa, P. Huttunen and M.A. Herman, *J. Appl. Phys.* **54**, 6047 (1983).
9. C. H. L. Goodman and M. V. Pessa, *J. Appl. Phys.* **60**, R65 (1986).
10. M. A. Herman, M. Valli and M. Pessa, *J. Cryst. Growth* **73**, 403 (1985).
11. V. P. Tanninen, M. Oikkonen and T. Tuomi, *Phys. Status Solidi A* **67**, 573 (1981).
12. V. P. Tanninen, M. Oikkonen and T. Tuomi, *Thin Solid Films* **90**, 283 (1983).
13. D. Theis, H. Oppolzer, G. Etchinghaus and S. Schild, *J. Cryst. Growth* **63**, 47 (1983).
14. S. Lin, *J. Electrochem. Soc.* **122**, 1405 (1975).
15. H. Antson, M. Leskela, L. Niinisto, E. Nykanen and M. Tammenmaa, *Kem.-Kemi* **12**, 11 (1985).
16. R. Tornqvist, Ref. 57 in the bibliography of Chapt. 1 of Ref. 39 of this report.
17. M. Ylilammi, M. Sc. Thesis, Helsinki Univ. of Technology, Espoo (1979).
18. L. Hiltunen, M. Leskela, M. Makela, L. Niinisto, E. Nykanen and P. Soininen, *Surface Coatings and Technology*, in press.
19. I. Suni, Ref. 66 in the bibliography of Chapt. 1 of Ref. 39 in this report.
20. S. M. Bedair, M. A. Tischler, T. Katsuyama and N.A. El-Masry, *Appl. Phys. Lett.* **47**, 51 (1985).
21. M. A. Tischler and S. M. Bedair **48**, 1681 (1986).
22. M. A. Tischler and S. M. Bedair, *J. Cryst. Growth* **77**, 89 (1986).
23. M. A. Tischler, N. G. Anderson and S.M. Bedair, *Appl. Phys. Lett.* **49**, 1199 (1986).
24. M. A. Tischler, N. G. Anderson, R.M. Kolbas and S.M. Bedair, *Appl. Phys. Lett.* **50**, 1266 (1987).
25. B.T. McDermott, N. A. El-Masry, M. A. Tischler and S.M. Bedair, *Appl. Phys. Lett.* **51**, 1830 (1987).
26. M. A. Tischler, N. G. Anderson, R. M. Kolbas and S. M. Bedair, *SPIE Growth Comp. Semicond.* **796**, 170 (1987).
27. S. M. Bedair in *Compound Semiconductor Growth Processing and Devices for the 1990's*, Gainesville, FL, 137 (1987).
28. J. Nishizawa, H. Abe and T. Kurabayashi, *J. Electrochem. Soc.* **132**, 1197 (1985).
29. M. Nishizawa, T. Kurabayashi, H. Abe, and N. Sakurai, *J. Electrochem. Soc.* **134**, 945 (1987).
30. P. D. Dapkus in Ref. 27, p. 95.
31. S. P. Denbaars, C.A. Beyler, A. Hariz and P.D. Dapkus, *Appl. Phys. Lett.* **51**, 1530 (1987).

32. M. Razeghi, Ph. Maurel, F. Omnes and J. Nagle, *Appl. Phys. Lett.* **51**, 2216 (1987).
33. M. Ozeki, K. Mochizuki, N. Ohtsuka and K. Kodama, *J. Vac. Sci. Technol.* **B5**, 1184 (1987).
34. Y. Suda, D. Lubben, T. Motooka and J. Greene, *J. Vac. Sci. Technol.* **B7**, 1171 (1989).
35. J. Nishizawa, K. Aoki, S. Suzuki and K. Kikuchi, *J. Cryst. Growth* **99**, 502 (1990).
36. T. Tanaka, T. Fukuda, Y. Nagasawa, S. Miyazaki and M. Hirose, *Appl. Phys. Lett.* **56**, 1445 (1990).
37. T. Suntola and J. Hyvarinen, *Ann. Rev. Mater. Sci.* **25**, 177 (1985).
38. M. Simpson and P. Smith, *Chem. Brit.* **23**, 37 (1987).
39. T. Suntola and M. Simpson, *Atomic Layer Epitaxy*, Chapman and Hall, New York, 1990.

## II. Routes to Chemically Self-Limiting ALE of SiC

### A. Introduction

The possibility of achieving an atomic layer epitaxial (ALE) process for SiC which is self limiting in some fashion hinges on the proper choice of the precursors for the process. Layer-by-layer processes for the ALE of SiC have been demonstrated but all require the judicious selection of the flow rates (exposures) of the silicon and carbon species to prevent the codeposition of silicon or graphite with the SiC [1,2]. Two factors are responsible for this problem. First, readily available silicon sources such as silane and disilane exhibit self-limiting adsorption characteristics only at low temperatures (25-400°C). At these temperatures, silane and disilane adsorb as  $\text{SiH}_x$  species and limit further adsorption by saturating all possible adsorption sites. At higher temperatures, hydrogen starts to desorb generating new adsorption sites and wrecking the self limiting adsorption characteristics [3-5]. This brings to point the second hindering factor to the self-limiting ALE of SiC which is the ability of adsorbed hydrogen on Si (100) to block adsorption sites for unsaturated hydrocarbons. Unlike saturated hydrocarbons which have been demonstrated to have a zero sticking coefficient on Si (100) [6], unsaturated hydrocarbons such as acetylene, ethylene, and propylene have been found to adsorb to Si (100) in approximately the same temperature range as silane and disilane on Si (100) [7-9]. Unfortunately, it has also been found that adsorbed hydrogen on Si (100) prevents any adsorption of these molecules on Si (100). Thus achieving a self limiting ALE of SiC with combinations of these readily available molecules seems doubtful.

Two precursors which have shown promise for leading to the achievement of a self-limiting SiC ALE are hexachlorodisilane ( $\text{Si}_2\text{Cl}_6$ ) and atomic hydrogen [10].  $\text{Si}_2\text{Cl}_6$  has been successfully used in combination with disilane ( $\text{Si}_2\text{H}_6$ ) to achieve the ALE of silicon and shown to exhibit chemically self limiting adsorption characteristics onto hydrogen terminated surfaces up to 500°C. As the adsorption of  $\text{Si}_2\text{H}_6$  onto chlorine terminated silicon was not self limiting, the entire ALE scheme itself was not a self limiting process. However, the use of atomic hydrogen to remove chlorine from a silicon surface, thus, allowing further adsorption of  $\text{Si}_2\text{Cl}_6$  has been demonstrated to lead to an entirely self limiting silicon ALE process [11]. Also of note is that Yates *et al.* have demonstrated that the interaction of atomic hydrogen with adsorbed methyl iodide on Si (100) results in quick and efficient removal of iodine but removes carbon at a rate which decreases with increasing temperature ( $T > 450\text{K}$ ) [12]. These results indicate that the combination of  $\text{Si}_2\text{Cl}_6$ , atomic hydrogen, and a carbon source could lead to an ALE process with some self-limiting characteristics.

The objective of this research is to find a suitable set of silicon and carbon precursors which both exhibit compatible self limiting adsorption characteristics which can be used to achieve a self limiting ALE of SiC. In this reporting period, the adsorption of  $\text{Si}_2\text{Cl}_6$  on clean

Si (100) and Si (100) saturated with acetylene and ethylene has been investigated using XPS and LEED. Similarly, the adsorption of acetylene and ethylene on clean Si (100) and chlorine terminated Si (100) has also been investigated. In addition, a hot filament atomic hydrogen source which is incased in a liquid nitrogen-cooled Teflon shroud has been designed, built, and installed for the purpose of removing chlorine from silicon surfaces without recourse to temperatures above 475°C.

## B. Experimental

*NCSU Integrated Surface Science Facility.* All experiments were conducted in an integrated surface science system which consists of several independent UHV (ultra-high vacuum) systems connected to one another via a 36" UHV sample transfer line. The transfer line is independently pumped by a cryopump (CTI CryoTorr 8) and has a base pressure of  $2 \times 10^{-9}$  Torr. To date, this integrated UHV system incorporates a plasma cleaning chamber, a chamber for *in-situ* Raman, an angle resolved-ultraviolet photoelectron spectroscopy (AR-UPS) system, a molecular beam epitaxy (MBE) system, an analysis station for performing Auger electron spectroscopy and low energy electron diffraction (LEED), an atomic layer epitaxy (ALE) system, and an x-ray photoelectron spectroscopy (XPS) system. The experiments discussed in this report employ only the XPS, ALE, and LEED systems.

*ALE system.* The ALE system consists of a stainless steel UHV chamber pumped by a 500 l/s ion pump (Varian), 360 l/s turbomolecular pump (Leybold), and a water cooled titanium sublimation pump. The base pressure in this system is  $3 \times 10^{-10}$  Torr. The ALE system is equipped with a HAL 201 quadrupole mass spectrometer (Hiden Analytical Ltd.), separate gas dosers for both hexachlorodisilane, acetylene, and ethylene, and a sample heating stage. The gas dosers employed are of the design of Yates *et al.* [13] and utilize a five micrometer diameter orifice laser drilled in a VCR gasket (Precision Laser Services) through which the gases were allowed into the system. Collimation of the gases into a "molecular beam" focused onto the sample was achieved using a 13 mm diameter, 2 mm thick glass capillary array with a ten micrometer pore size (Galileo Electro Optics). The sample heating stage consists of a wound tungsten filament mounted on a boron nitride disk supported by four alumina tubes connected to the bottom of a cup shaped molybdenum sample holder (see Fig. 1). The tungsten filament is positioned in close proximity to the back of the sample allowing for efficient heating of the sample. Heating profiles are controlled by measuring the temperature of the back of the wafer using a K-type thermocouple mounted directly behind the sample and a Eurotherm 818P programmable heater controller and a Eurotherm 830 20 amp SCR power supply. Surface temperatures are measured using a Minolta/Land Cyclops 52 infrared thermometer. The mass spectrometer is housed in a separate differentially pumped cylindrical chamber similar in design to that of Smentkowski and Yates [14]. The chamber has a .5 cm

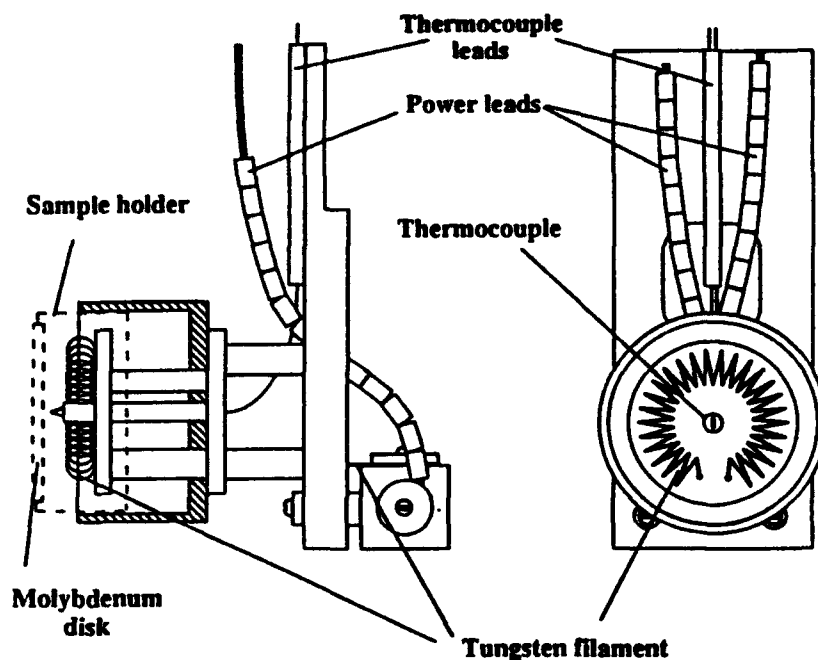


Figure 1. Design of the sample mounting/heating stage. Heating is provided by the tungsten filament in close proximity to the back of the molybdenum disk. The temperature is measured by chromel-alumel thermocouple. The dashed lines represent the sample holder and disk on which the silicon sample is mounted.

diameter orifice at the head of the QMS for performing TPD (Temperature Programmed Desorption) experiments and an approximately 50 cm<sup>2</sup> "sunroof" which can be opened for monitoring residual gases in the system. The system pressure is monitored using a Granville Phillips Series 271 ionization gauge.

*XPS system.* XPS experiments are performed in a stainless steel UHV chamber pumped by a 220 l/s ion pump (Varian) equipped with a VG XR3E2 x-ray source and VG CLAM II hemispherical electron energy analyzer. This system is also equipped with a VG LEG 62 electron gun for performing Auger electron spectroscopy and a computer driven sample stage with 5 degrees of freedom for looking at Auger electron/photoelectron forward scattering and diffraction. The base pressure in this system is  $1 \times 10^{-10}$  Torr as monitored by a Granville Phillips Series 271 ionization gauge and never rises above  $8 \times 10^{-10}$  Torr during typical XPS analysis. All XPS spectrums reported here were taken using Al K alpha radiation (1486.6 eV). Calibration of the binding energy scale for all scans was achieved by periodically taking scans of the Au 4f<sup>7/2</sup> and Cu 2p<sup>3/2</sup> peaks from standards and correcting for the discrepancies in the measured and known values of these two peaks (83.98 eV and 932.67 eV respectively). Curve fitting of most data was performed using the software package GRAMS 386. A combination Gaussian-Lorentzian curve shape with a linear background was found to best represent the data.

**LEED.** The low energy electron diffraction optics (Perkin-Elmer) are mounted on a cross off the transfer line and pumped through this line.

**Substrate cleaning.** In these experiments, one-inch diameter n-type Si (100) wafers with 1 ohm-cm resistance obtained from Virginia Semiconductor were used as substrates. Prior to insertion into vacuum, all wafers were given a standard UV-HF spin treatment after which the wafers were fastened to a ring shaped molybdenum sample holder using tantalum wire. Once in vacuum, the silicon wafers were inserted in the ALE systems where they were outgassed at 250°C for 45 min., annealed at 850°C for 10 min., 950°C for 1min and then slowly cooled to room temperature. This resulted in a sharp well ordered 2×1 low energy electron diffraction (LEED) pattern. XPS of wafers undergoing this cleaning procedure showed only trace amounts of oxygen and carbon.

**Gases and Gas Dosing.** Hexachlorodisilane ( $\text{Si}_2\text{Cl}_6$ ) was purchased from Cambridge Isotopes and contained in a 70 cc stainless steel sample cylinder connected to the ALE system via the gas dosing manifold. The  $\text{Si}_2\text{Cl}_6$  was purified by repeated freeze-pump-thaw cycles until mass spectroscopic analysis of the  $\text{Si}_2\text{Cl}_6$  revealed that no impurities existed. As  $\text{Si}_2\text{Cl}_6$  is a liquid with a vapor pressure of 1-3 Torr at room temperature, a small amount (.5 Torr as measured by a MKS type 127A Baratron Capacitance Manometer) of the  $\text{Si}_2\text{Cl}_6$  vapor was allowed to expand through the 5 micrometer orifice of the dosing apparatus for a given period of time.

Purified acetylene was obtained from the acetylene purification system installed on the SiC layer by layer growth system and has been described in a previous report. Mass spectroscopic analysis of the purified acetylene did not show any of the signatures characteristic of acetone which the acetylene had been previously dissolved in. However, a significant impurity at m/e #28 was detected which could be a result of either nitrogen or carbon monoxide. As direct reaction of the purified acetylene with Si (100) at temperatures from 25°C to 1000°C did not show any presence of oxygen or nitrogen in XPS analysis, it was felt that the impurity was relatively inert for the experiments reported here which were maintained below 475°C. However, the inability to clarify the identity of this impurity prompted switching to ethylene as a carbon source in later experiments. The ethylene was purchased from Air Products and did not reveal any detectable impurities in mass spectroscopic analysis. Acetylene and ethylene dosing was handle in a manner exactly analogous to that in which the  $\text{Si}_2\text{Cl}_6$  was handled.

### C. Results

**$\text{Si}_2\text{Cl}_6$  adsorption on Si (100).** Figure 2 shows several scans of the Cl LMM x-ray excited Auger electron peak on Si (100) after sequential exposures to  $\text{Si}_2\text{Cl}_6$  at 475°C. The Cl LMM peak was found to be the best feature to monitor in XPS spectrums when looking at  $\text{Si}_2\text{Cl}_6$  adsorption on Si (100). This was mainly due to the weaker intensities of the Cl  $2p^{3/2,1/2}$  and

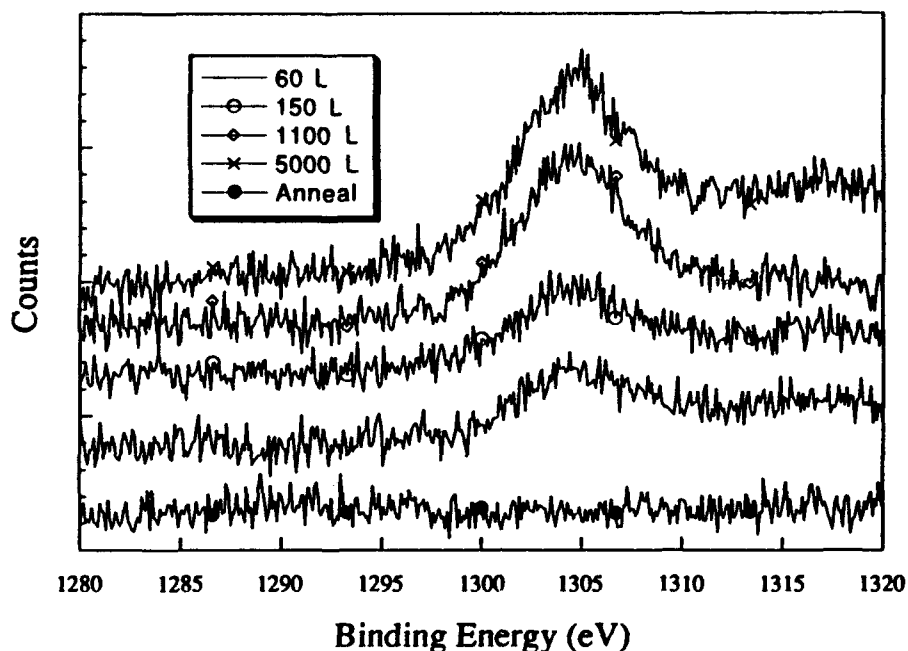


Figure 2. XPS spectrum of the Cl LMM x-ray excited photoelectron peak from a Si (100) wafer after various sequential exposures to hexachlorodisilane ( $\text{Si}_2\text{Cl}_6$ ). The bottom scan is from the wafer after cleaning/annealing but before exposure to  $\text{Si}_2\text{Cl}_6$ .

other Cl photoelectrons and due to the inability to distinguish between silicon from  $\text{Si}_2\text{Cl}_6$  and silicon from the wafer. Looking at the first spectrum taken after 60 L  $\text{Si}_2\text{Cl}_6$ , one can readily see the Cl LMM peak indicating efficient adsorption of the  $\text{Si}_2\text{Cl}_6$  on the silicon wafer. The second scan shows a corresponding rise in the Cl LMM intensity which tapers off in the third and fourth scans from extremely large exposures. This leveling off in Cl LMM intensity can be taken to indicate that  $\text{Si}_2\text{Cl}_6$  adsorption on Si (100) is self limiting. After the final  $\text{Si}_2\text{Cl}_6$  exposure, a diffuse (1×1) LEED pattern was obtained indicating that the Si-Si dimer bonds present at the start of the  $\text{Si}_2\text{Cl}_6$  exposure had been broken via the  $\text{Si}_2\text{Cl}_6$ .

*C<sub>2</sub>H<sub>2</sub> and C<sub>2</sub>H<sub>4</sub> adsorption on Cl-Si (100).* In order to investigate the direct reaction of acetylene and ethylene with Cl terminated Si (100), two silicon wafers were pre-exposed to > 5000 L  $\text{Si}_2\text{Cl}_6$  which again produced a diffuse (1×1) LEED pattern. These two wafers then were exposed to saturation doses (>10,000L) of acetylene and ethylene at 475°C. XPS analysis of the two wafers after exposure to the hydrocarbons showed only a slight decrease in the CL LMM intensity (as shown in Fig. 3 for the acetylene exposed wafer) and a marginal increase in the C 1s signal. Owing to the long time of the exposures >10 min., the small decrease in the Cl LMM intensity can be attributed to thermal desorption at 475°C rather than reaction with acetylene or ethylene.

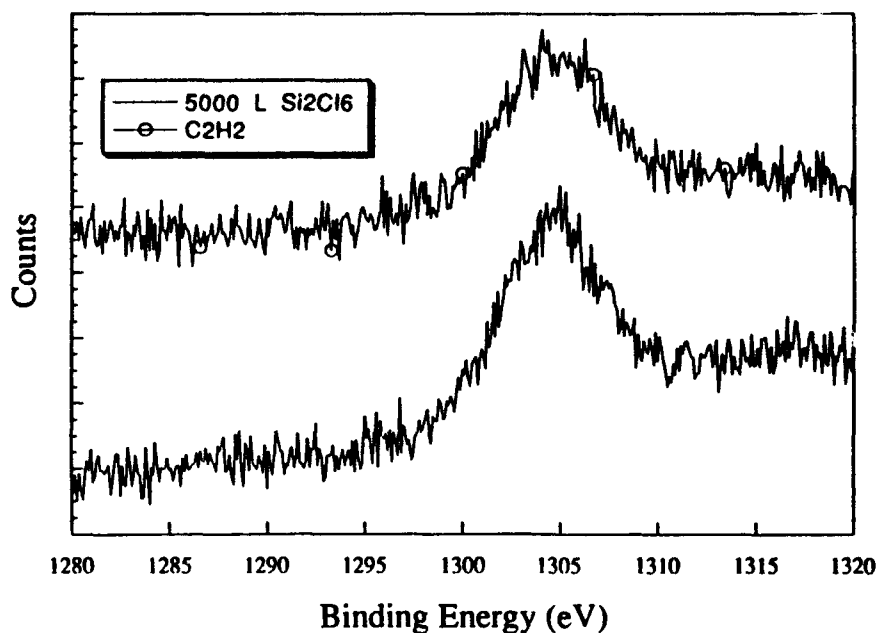


Figure 3. XPS spectrums of Cl LMM from chlorine terminated Si (100) before and after exposure to acetylene.

*Si<sub>2</sub>Cl<sub>6</sub> adsorption on hydrocarbon terminated Si (100).* In order to investigate the ability of Si<sub>2</sub>Cl<sub>6</sub> to directly react with a hydrocarbon terminated surface, one silicon wafer was saturated with acetylene and another with ethylene (both at room temperature and > 10,000L). The acetylene saturated wafer was then exposed to >1000L of Si<sub>2</sub>Cl<sub>6</sub> at 475°C. The ethylene saturated wafer was exposed to Si<sub>2</sub>Cl<sub>6</sub> at 250°C to avoid desorption of the ethylene [15]. Figure 4 shows an XPS scan of the Cl LMM from the acetylene saturated silicon wafer both before and after Si<sub>2</sub>Cl<sub>6</sub> exposure. It is readily apparent that Cl is present on the surface after Si<sub>2</sub>Cl<sub>6</sub> exposure indicating decomposition of the Si<sub>2</sub>Cl<sub>6</sub> on the surface. From this data it is difficult to say with full confidence whether the Si<sub>2</sub>Cl<sub>6</sub> reacted with the carbon on the surface to form Si-C bonds or adsorbed on sites on the silicon wafer unoccupied by the hydrocarbons.

#### D. Discussion

The XPS results on Si<sub>2</sub>Cl<sub>6</sub> adsorption on Si (100) at 475°C shows that this step is self limiting as has also been shown by Gates et al [10,11]. However in order for this step to remain self limiting, a temperature ceiling of 475-525°C must be imposed so as to avoid desorption of chlorine which becomes more rapid at higher temperatures and could lead to etching. Since it has been shown that hydrocarbons will not adsorb/react with a chlorine terminated silicon surface, some means of removing chlorine from the silicon surface after Si<sub>2</sub>Cl<sub>6</sub> adsorption must be employed in order to enable the possible adsorption of hydrocarbons. The method of chlorine removal must not in any way alter the self limiting characteristics of the Si<sub>2</sub>Cl<sub>6</sub> adsorption and should allow for an isothermal process. For these

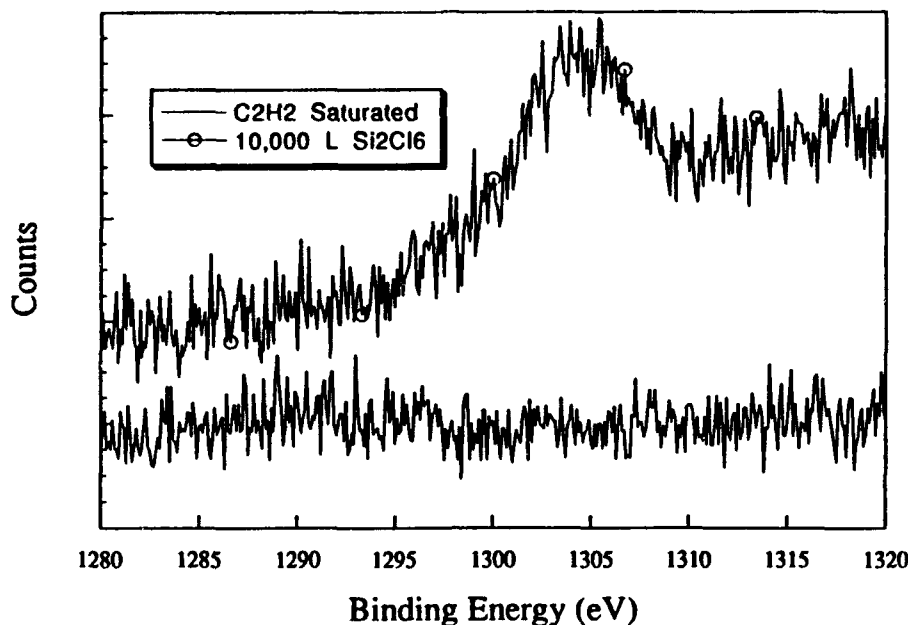


Figure 4. XPS spectra of Cl LMM from hydrocarbon terminated Si (100) both before and after exposure to  $\text{Si}_2\text{Cl}_6$ .

reasons, thermal desorption of the chlorine is not favorable. A better idea is to use atomic hydrogen to remove the chlorine from the surface which would not interfere with the adsorption characteristics of the  $\text{Si}_2\text{Cl}_6$  and would allow for an isothermal process.

Yates *et al.* [12] have already demonstrated the ability of atomic hydrogen to remove halogens from silicon surfaces via an Ely-Rideal process and Koleske *et al.* [11] have already demonstrated atomic hydrogen to be useful in the ALE of silicon using  $\text{Si}_2\text{Cl}_6$ . To this end, a hot filament (atomic hydrogen source) which is surrounded by a liquid nitrogen-cooled Teflon shroud has been commissioned. The purpose of the liquid nitrogen shroud is to avoid heating the sample with the hot the rhenium filament as well as avoiding any evaporation of rhenium onto the silicon wafer. The shroud is made of Teflon as the author has been advised that atomic hydrogen does not react with or recombine on Teflon at liquid nitrogen temperatures [16]. The liquid nitrogen-cooled shroud has been built, tested, and deemed UHV compatible. Testing of the shroud and hot filaments ability to produce atomic hydrogen is eminent.

#### E. Conclusion

At  $475^\circ\text{C}$ ,  $\text{Si}_2\text{Cl}_6$  readily adsorbs on clean Si (100) surfaces in a chemically self limiting fashion. Si (100) surfaces exposed to saturation doses of acetylene and ethylene show the presence of chlorine after exposure to  $\text{Si}_2\text{Cl}_6$ . Exposure of chlorine terminated Si (100) surfaces to large doses of acetylene and ethylene shows little removal of chlorine and only a minute increase in carbon concentration at the silicon surface. This indicates that chlorine

effectively acts to cap possible adsorption sites on the silicon surface in a manner analogous to what Yates *et al.* [10] have demonstrated to be the case for pre adsorbed hydrogen on silicon. Therefore, if chemically self-limiting ALE of SiC using Si<sub>2</sub>Cl<sub>6</sub> and a hydrocarbon is to be achieved, an intermediate step must be introduced in which atomic hydrogen is used to remove chlorine from the silicon surface prior to adsorption of the hydrocarbon.

#### F. Future Research

1. Test the ability of a hot filament-atomic hydrogen source to remove chlorine from Si (100) when the filament is surrounded by a liquid nitrogen-cooled Teflon shroud.
2. Compare the efficiency of removing chlorine from Si (100) using atomic hydrogen from an unshielded hot filament and atomic hydrogen from a hot filament in a liquid nitrogen cooled Teflon shroud.
3. Try to grow SiC at 475°C using a repeated growth sequence of Si<sub>2</sub>Cl<sub>6</sub>, atomic hydrogen, and ethylene.

#### G. References

1. T. Fuyuki, M. Nakayama, T. Yoshinobu, H. Shiomi, H. Matsunami, *J. Crystal Growth*, **95**, 461, (1989).
2. S. Hara, Y. Aoyagi, M. Kawai, S. Misawa, E. Sakuma, S. Yoshida, *Surface Science*, **273**, 437 (1992).
3. D. Lubben, R. Tsu, T.R.Bramblett, J. E. Greene, *J. Vac. Sci. Technol.*, **A9**, 3003 (1991).
4. S. K. Kukarni, S. M. Gates, C. M. Greenlief, H. H. Sawin, *J. Vac. Sci. Technol.*, **A8**, 2956 (1990).
5. S. M. Gates, *Surface Science*, **195**, 307 (1988).
6. M. J. Bozack, P. A. Taylor, W. J. Choyke, J. T. Yates Jr., *Surface Science*, **177**, L933 (1986).
7. J. Yoshinobu, H. Tsuda, M. Onchi, M. Nishijima, *J. Chem. Phys.* **87**, 7332 (1987).
8. M. J. Bozack, W. J. Choyke, L. Muehlhoff, J. T. Yates Jr., *J. Appl. Phys.* **60**, (1986).
9. C. C. Cheng, W. J. Choyke, J. T. Yates Jr., *Surface Science* **231**, 289, (1990).
10. D. D. Koleske, S. M. Gates, D. B. Beach, *J. Appl. Phys.*, **72**, (1992).
11. D. D. Koleske, S. M. Gates, *Appl. Phys. Lett.* **64** (7), 884 (1994).
12. C. C. Cheng, S. R. Lucas, H. Gutleben, W. J. Choyke, J. T. Yates, *Surface Science* **273**, L441, (1992).
13. M. J. Bozack, L. Muehlhoff, J. N. Russel Jr., W. J. Choyke, J. T. Yates Jr., *J. Vac. Sci. Technol.* **A5**, 1 (1987).
14. V. S. Smentkowski and J. T. Yates Jr., *J. Vac. Sci. Technol.* **A7**, 3325, (1989).
15. C. C. Cheng, W. J. Choyke, J. T. Yates, *Surface Science* **231**, 289 (1990).
16. Personal communication with Dr. J. T. Yates at University of Pittsburgh.

### III. Layer-by-Layer Deposition of SiC Thin Films: Growth, Characterization and Device Development

#### A. Introduction

The potential of SiC for enhancing the capabilities of semiconductor devices is reflected by its Johnson and Keyes figures of merit. Johnson's figure of merit rates the maximum performance to be expected of a semiconductor material in discrete bipolar transistors[1], giving  $\beta$ -SiC a rating 33.9 times higher than Si, largely due to an  $E_B(\beta\text{-SiC})$  that is 13.3 times higher than that of Si. Keyes rating, which assesses a materials suitability for high density integrated circuit applications[2] rates  $\beta$ -SiC 5.82 times higher than Si due to the superior value of  $\sigma_T(\beta\text{-SiC})$  that is 1.22 times that of copper at room temperature[3]. These ratings for SiC demonstrate that both discrete devices and integrated circuitry employing SiC components should attain levels of performance unachievable with device technologies based solely on Si.

Although many successful SiC-based devices have been produced[4,5], SiC-based microelectronic technology is still in its infancy, especially when compared to Si-based technology. The most expeditious route to devices exploiting the performance increases possible with SiC would be the development of a thin-film deposition technique to allow the integration of  $\beta$ -SiC into the existing Si device fabrication infrastructure. However, the incorporation such a deposition step into an integrated circuit or device fabrication procedure would be very difficult since monocrystalline deposition of SiC on a Si(100) substrate typically occurs in two steps. Firstly, an off-axis wafer is exposed to a C-containing gas species to carbonize the surface to a thickness of 150-300Å. This SiC conversion layer is subsequently exposed to both Si- and C-containing gases at  $\approx 1350^\circ\text{C}$  to form much thicker  $\beta$ -SiC films[6]. Neither the carbonizing nor the high temperature steps can be easily integrated into current sub-micron Si process routes and the lack of a technology that allows the incorporation of SiC thin film processing routes into the existing Si device and integrated circuit infrastructure is a substantial barrier to the wider use of devices making use of  $\beta$ -SiC films. However, with low deposition temperatures atomic layer epitaxy offers the ability to eliminate both process difficulties and may serve as a vehicle to facilitate the use of SiC in selected devices.

The objective of this research is to extend the state-of-the-art regarding SiC thin film deposition and application via the employment of atomic layer epitaxy (ALE) to deposit  $\beta$ -SiC films on select substrates. During this reporting period work has continued toward the fabrication of trenched heterojunction bipolar transistors (HBTs) employing a wide bandgap  $\beta$ -SiC emitter. This work has included: optimization of deposition parameters including deposition within trenches etched into Si(100) wafers, electrical characterization of unintentionally n-type and Al doped p-type monocrystalline  $\beta$ -SiC films, developing the ability to form and photolithographically pattern ohmic contacts to n-type  $\beta$ -SiC and the design and

fabrication of photolithography contact masks. The following sections describe the experimental procedures and the results and provide a discussion and conclusions regarding the research conducted in this period.

## B. Experimental Procedure

*ALE Reactor.* The ALE reactor employed in this research has not been significantly modified since it was described in detail in a previous report (June, 1993). To prevent mixing of process gases, flowing Ar "curtains" divide the reactor into 4 radial quadrants through which isolated fluxes of Si<sub>2</sub>H<sub>6</sub>, C<sub>2</sub>H<sub>4</sub>, NH<sub>3</sub> and triethylaluminum (Al(C<sub>2</sub>H<sub>5</sub>)<sub>3</sub>) may flow. The quadrant containing NH<sub>3</sub> also contains a W filament that may be heated to produce atomic hydrogen or to crack NH<sub>3</sub> depending on gas flow conditions. During deposition, heated samples can be rotated alternately between quadrants and exposed to the species present to form films in a layer-by-layer process. Due to the construction of the reactor, SiC films can be deposited and doped n and p-type with N and Al, respectively.

*Preparing Substrates.* Three kinds of wafer substrates were employed in this research: A) As doped (10<sup>19</sup> cm<sup>-3</sup>), n-type Si(100) oriented off-axis 3° toward <110>; B) doped (10<sup>17</sup> cm<sup>-3</sup>), p-type Si(100); and C) N doped (10<sup>17</sup> cm<sup>-3</sup>), n-type α-6H-SiC(0001) oriented off-axis 3.5° toward <11 $\bar{2}$ 0>. The α-6H-SiC(0001) substrates were received with ≈750 Å of SiO<sub>2</sub> grown on the surface so these substrates were immersed in a 10% HF solution for 5 minutes before loading into the system. Si(100) substrates were loaded into the system immediately after RCA cleaning.

*Trenched Si(100) Substrates.* Trenched Si substrates were produced from the n-type Si(100) wafers using conventional semiconductor fabrication techniques. Wafers were thermally oxidized according to a dry-wet-dry recipe at 950°C to form ≈5000 Å of SiO<sub>2</sub> which was photolithographically patterned using a custom mask. A series of parallel strips of Si were uncovered by dipping in HF. Using the SiO<sub>2</sub> pattern, the wafers were reactive ion etched at 100 watts in an atmosphere formed by flowing 15 and 12.5 sccm of SF<sub>6</sub> and O<sub>2</sub>, respectively to form the trenches. The remaining SiO<sub>2</sub> was removed using an HF dip.

*P-type SiC(100) films.* The Al dopant for the deposition of p-type β-SiC films was obtained from a conventional organometallic bubbler containing triethylaluminum (TEAl). During deposition the TEAl was held at 62°C, creating a vapor pressure of 1 Torr and entrained in H<sub>2</sub> flowing at 150 sccm as the total bubbler pressure was maintained at 300 Torr. The amount of TEAl supplied to the growing film was controlled by the residence time spent in the TEAl flux.

*Deposition.* Silicon carbide films were deposited on the substrates by a sequential exposure to Si<sub>2</sub>H<sub>6</sub>, C<sub>2</sub>H<sub>4</sub> and atomic hydrogen. The deposition of p-type films was accomplished by exposing the sample to a very dilute flow of TEAl between each Si and C exposure. Optimal

growth conditions are described in Table I; note that there are two process steps for deposition on Si(100) substrates.

Table I. Optimal values of growth parameters

Process parameter	$\alpha(6H)$ -SiC(0001)	Si(100) Step 1	Si(100) Step 2
Sample temperature	900° C	850° C	900° C
Si <sub>2</sub> H <sub>6</sub> flow/ H <sub>2</sub> carrier	2 sccm	0.8 sccm/ 300 sccm	0.8 sccm
C <sub>2</sub> H <sub>4</sub> flow/ H <sub>2</sub> carrier	2 sccm	2 sccm/ 200 sccm	2 sccm
Ar curtain flow	0 sccm	200 sccm	0 sccm
H <sub>2</sub> across filament	≈ 1 sccm	100 sccm	≈ 1 sccm
Filament temperature	unheated	1800° C	unheated
Pressure	$5 \times 10^{-4}$ torr	1.5 torr	$5 \times 10^{-4}$ torr
Rotational Scheme	Under Si <sub>2</sub> H <sub>6</sub> 5 sec. Under fil. 30 sec. Under C <sub>2</sub> H <sub>4</sub> 5 sec. Under fil 5 sec. Repeat (61 sec./cycle)	Rotate from under fil. past Si <sub>2</sub> H <sub>6</sub> and C <sub>2</sub> H <sub>4</sub> without stopping. Under fil 30 sec. Repeat (41 sec./cycle)	Under Si <sub>2</sub> H <sub>6</sub> 5 sec. Under fil. 30 sec. Under C <sub>2</sub> H <sub>4</sub> 5 sec. Under fil 5 sec. Repeat (61 sec./cycle)

*Ni contacts (N-Type SiC).* Ni contacts were sputtered onto the films using either shadow mask or a photolithographic lift-off pattern. The specifics of the lift-off technique are pictured in Fig. 1. In 1B the wafer from 1A is coated with negative photoresist (Shipley positive photoresist + Imidizol®). After baking, this photoresist is patterned by ultraviolet exposure through a contact mask in 1C. Upon developing in 1D, an undercut forms as is characteristic of Imidizol®. In 1E the metal is applied, usually through vacuum evaporation, but in the case for Ni, sputtering is used. In 1F the photoresist is removed with Accustrip®. Sputtering conditions were power = 100 watts 13.56 MHz R.F. and 20 mtorr Ar ambient. Deposition rate was ≈ 2000 Å/Hr. Contacts were then annealed in a Heatpulse rapid thermal annealer (RTA) with an Ar ambient at 1000° C for 20 sec.

*Al contacts (P-type SiC).* Al contacts were vacuum evaporated from pure Al shot (99.9999% pure) using a shadow mask. Contacts were annealed in a Heatpulse RTA with an Ar ambient at 600° C for 60 sec.

### C. Results

*Optimizing deposition conditions.* Although it is possible to deposit monocrystalline  $\beta$ -SiC films on Si(100) using the previously developed layer-by-layer technique at 850°C, film quality improves significantly if the temperature is increased. However, high temperature deposition of

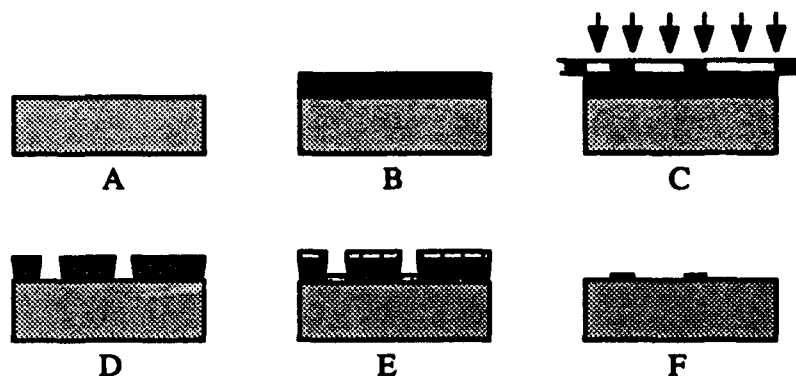


Figure 1. Photolithography lift-off technique.

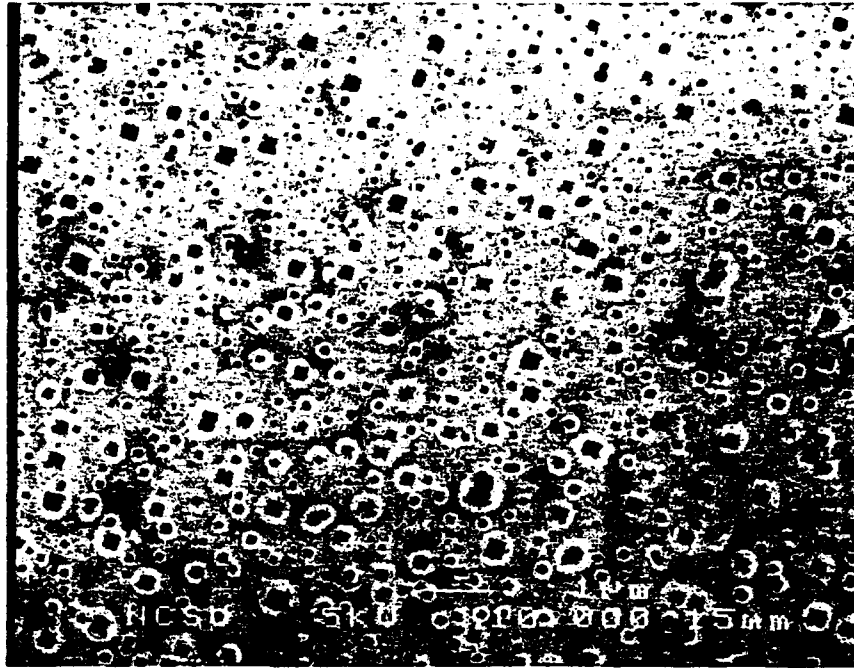
$\beta$ -SiC on Si(100) frequently results in pitting of the substrate as shown in Fig. 2, a high resolution transmission electron microscopy (HRTEM) image of a sample where the  $\beta$ -SiC film was deposited on a Si(100) substrate at 925°C. Chiu and Desu<sup>7</sup> have reported that during conversion of Si to SiC by a hydrocarbon gas, the reaction mechanism involves the diffusion of Si through the forming  $\beta$ -SiC film to react with the incident gas molecules and that defects in the  $\beta$ -SiC film serve as fast diffusion paths. As a consequence, it appears that in this work, with the low deposition rates employed, high temperature operation allows too much Si to diffuse out through a discontinuous  $\beta$ -SiC film pitting the substrate. To circumvent this difficulty, several low temperature "capping" layers of  $\beta$ -SiC were deposited at 850°C on Si(100) substrates prior to deposition at 925°C. Scanning electron microscopy (SEM) images of such samples prepared with capping layers of 10, 20, 50 and 100 cycles are shown in Fig. 3. Pitting is evident in all samples except for the sample with a 100 cycle capping layer, and this 100 cycle capping layer has become the first step of the optimal  $\beta$ -SiC/Si(100) deposition recipe.

Figures 4 and 5 are HRTEM images of  $\beta$ -SiC films deposited on Si(100) and  $\alpha$ (6H)-SiC(0001) substrates, respectively, using the optimized deposition parameters detailed in Table I. Ion milling damage is evident in the  $\beta$ -SiC/ Si(100) image as the amorphous appearing region at the  $\beta$ -SiC: Si interface. Stacking faults and twin defects are evident in both samples although stacking faults appear to be slightly less common in  $\beta$ -SiC films on Si(100) substrates.

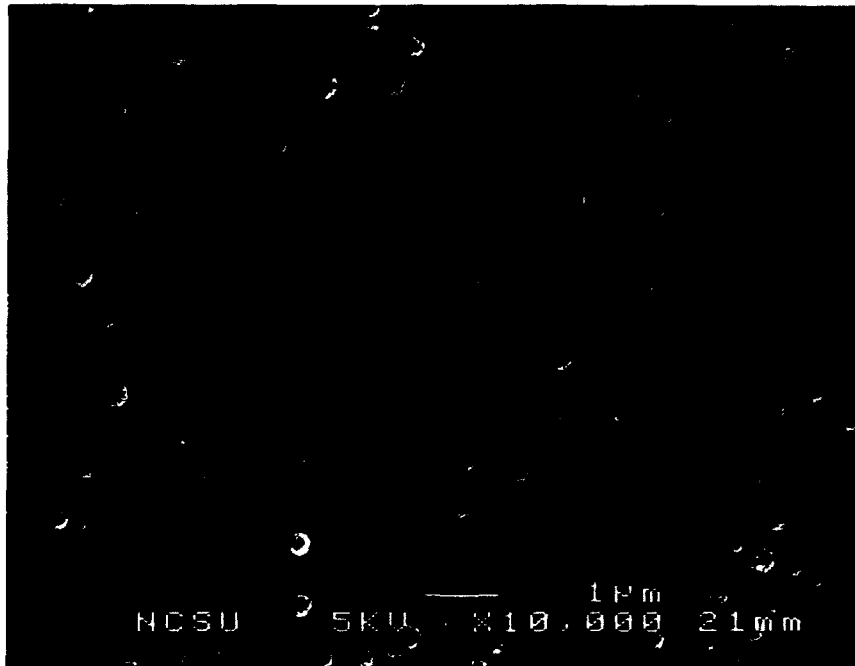
*Trenched Substrates.* Films have been deposited within trenches etched into Si(100) wafers using the optimized deposition recipe from Table I. The fabrication of the trenched wafers was described in the previous report (Dec. 1993). A typical  $\beta$ -SiC film deposited within a trench using the optimized  $\beta$ -SiC / Si(100) recipe is shown in Fig. 6. The pictured film is .83  $\mu\text{m}$  thick after 3850 cycles giving a deposition of .98 monolayers per cycle.



Figure 2. Pit in Si(100) substrate after high temperature deposition of  $\beta$ -SiC.

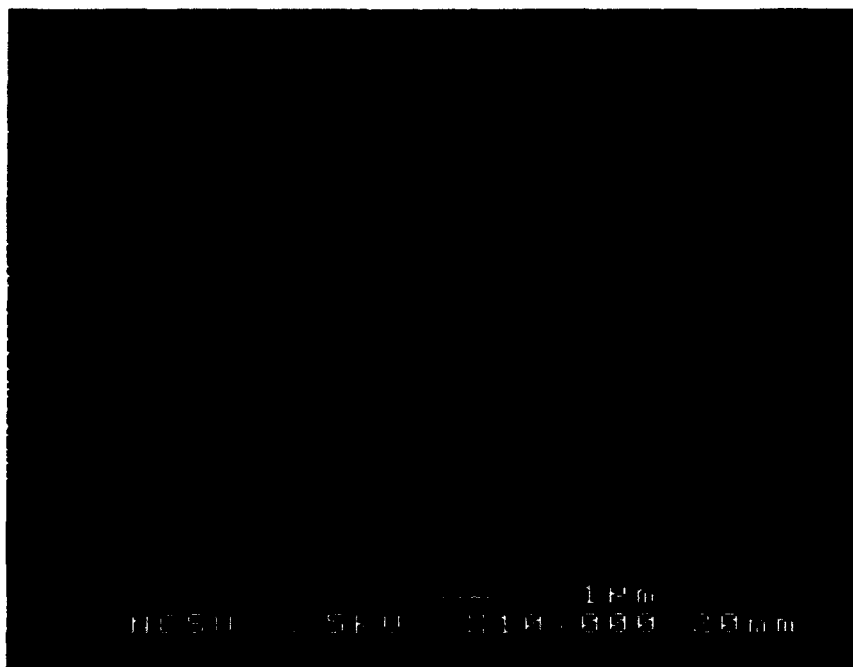


Cap by 10 cycles SiC

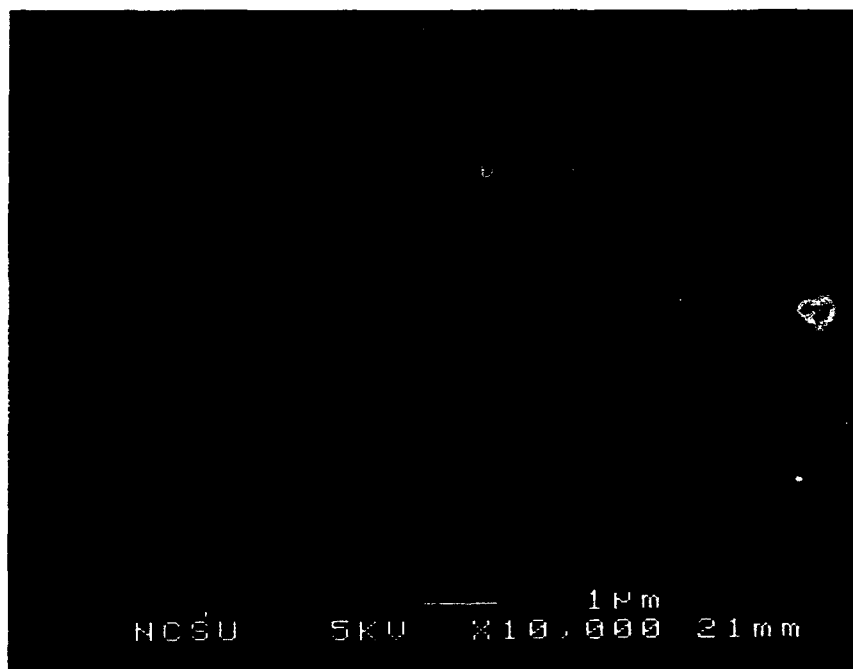


Cap by 20 cycles SiC

Figure 3. Reduction of pitting in Si(100) substrate at 925°C after capping with SiC at 850°C.



Cap by 50 cycles SiC



Cap by 100 cycles SiC

Figure 3 Con't. Reduction of pitting in Si(100) substrate at 925°C after capping with SiC at 850°C.

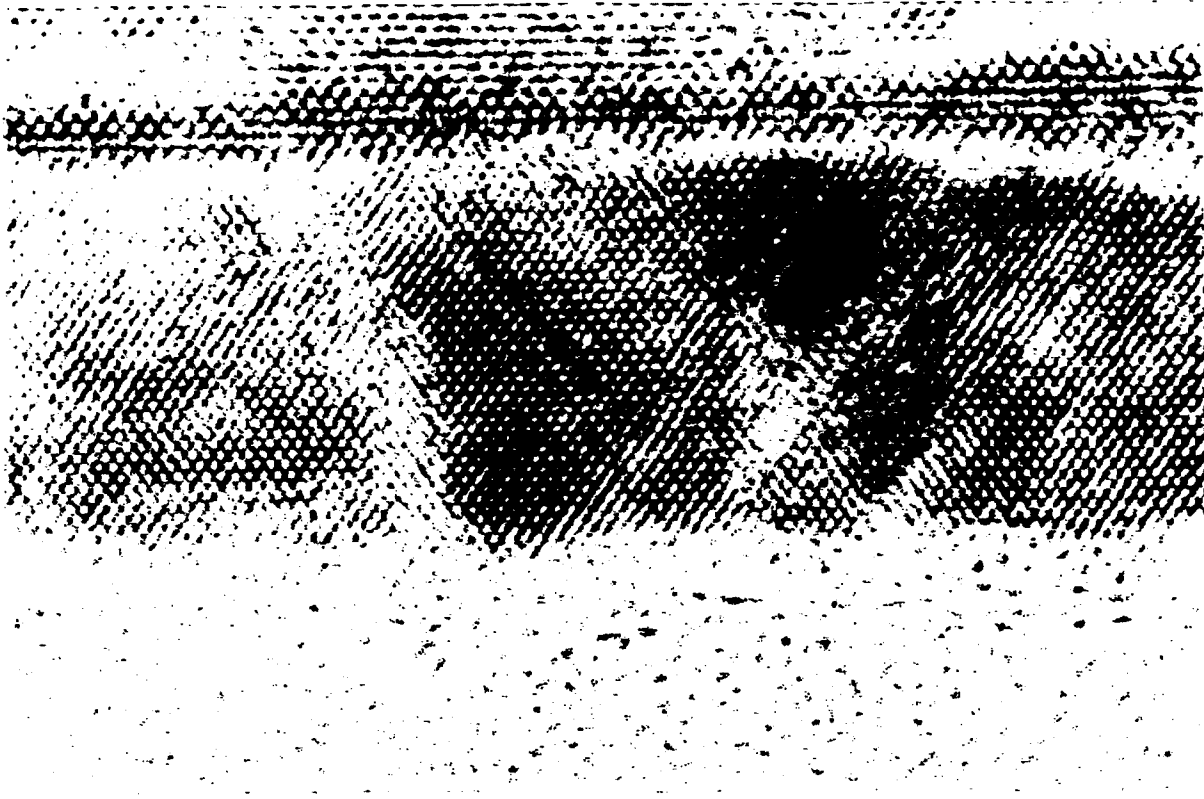


Figure 4. High resolution transmission electron micrograph of  $\beta$ -SiC film on Si(100) substrate.

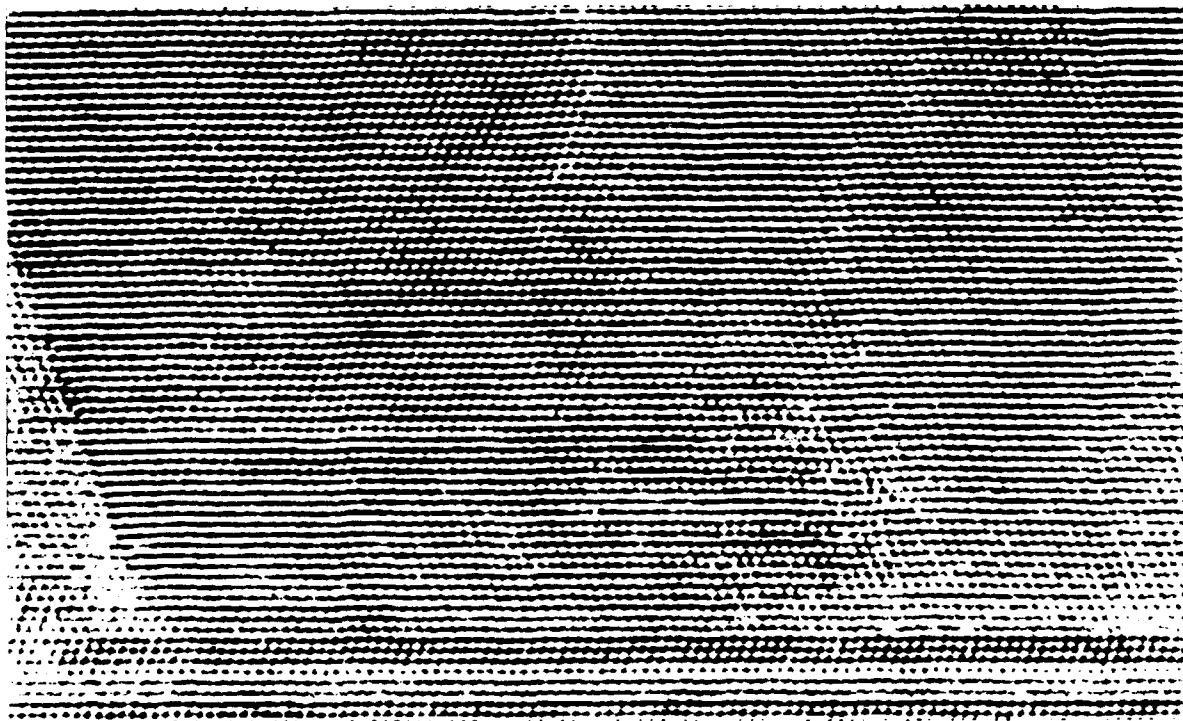


Figure 5. High resolution transmission electron micrograph of  $\beta$ -SiC film on  $\alpha(6H)$ -SiC(0001) substrate.

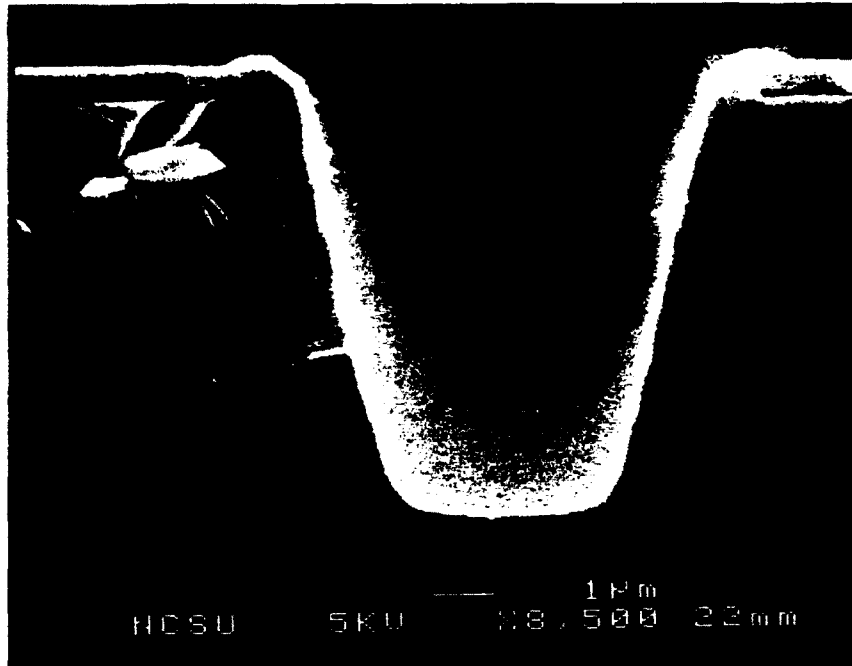


Figure 6.  $\beta$ -SiC film in trench on Si(100) substrate.

*Electrical contacts:* For electrical characterization by Hall mobility measurement and for future use in fabricating devices, it was necessary to develop the ability to form and pattern ohmic contacts to p and n-type  $\beta$ -SiC films. Ohmic behavior was characterized as shown in Fig. 7 by monitoring  $I$  vs.  $V_{\text{appl}}$ . If the contacts were ohmic, a linear I-V behavior is expected while a change in slope on going from negative to positive potential or non-linear behavior indicates a rectifying contact. Al contacts were vacuum evaporated to make the contacts to p-type films. Evaporated Al contacts were relatively ohmic as seen by the approximately linear I-V curve in Fig. 8. However annealing the contacts at  $600^\circ\text{C}$  for 60 sec.

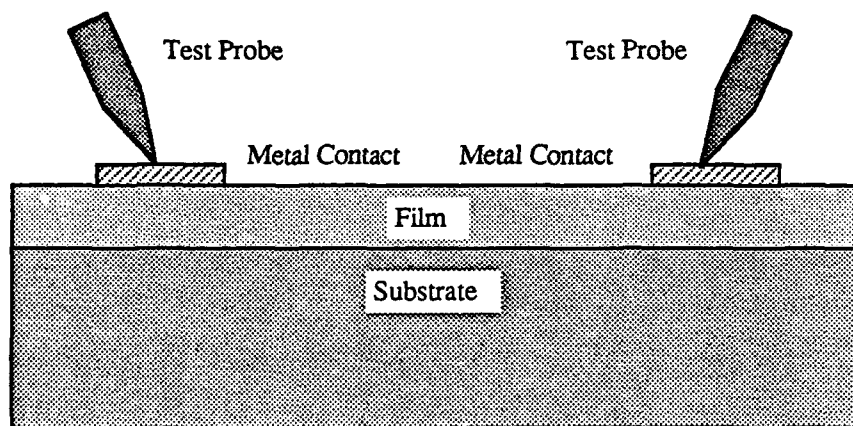


Figure 7. Testing contacts for ohmic behavior.

improved the linearity as seen when comparing Fig. 9, I-V curve of annealed Al contacts, to Fig. 8, I-V curve of as deposited Al contacts.

Ni contacts were also fabricated using a shadow mask, but the Ni was sputtered. Annealed Ni contacts made to n-type  $\beta$ -SiC were ohmic as seen in the corresponding I-V curve in Fig. 10. However, the contacts become increasingly rectifying when used on n-type  $\beta$ -SiC films of lower carrier concentrations.

*Lift-off technique.* The lift-off technique described in Fig. 1 was developed for patterning vacuum evaporated Al. Therefore no difficulty is expected in using this method to pattern the Al contacts on future devices. However the Ni is not evaporated but is sputtered instead. The lift-off technique described relies on shadowing of the inclined side-walls of the photoresist to allow later access to the exposed photoresist by a solvent. Vacuum evaporation is very anisotropic so shadowing is very effective. However sputtering is more isotropic and some material is deposited on the side-walls. Using the mask for trenching substrates as a template, it has been found that there is a maximum thickness of  $\approx 2,000\text{\AA}$  above which the lift-off technique will not work with sputtered Ni films. Fortunately  $2000\text{\AA}$  of Ni should be sufficient for the HBT contacts and patterned Ni lines  $2000\text{\AA}$  thick are pictured in Fig. 11.

*Electrical properties.* N- and p-type films grown on substrates of the opposite conductivity type have been examined based on Hall mobility and I-V behavior. Table II reports the data acquired from 2 n-type (N1 and N2) and 3 p-type films (P1, P2 and P3). The n-type films were deposited on p-type Si(100). N1 was deposited using the "old" recipe for  $\beta$ -SiC/ Si(100) [step 1 of the optimized  $\beta$ -SiC/ Si(100) process but run for a long time]. N2 used the full  $\beta$ -SiC/ Si(100) recipe from Table I. The p-type films P1, P2 and P3 were deposited on n-type  $\alpha(6H)$ -SiC(0001) substrates with differing exposures to TEAl and  $C_2H_4$  during each cycle. P1 was exposed to no  $C_2H_4$  and all of the C came from a 5 second exposure to TEAl. P2 was exposed to TEAl for 1 second and then to  $C_2H_4$  for 0.5 seconds while P3 was exposed to TEAl for 1 second and to  $C_2H_4$  for 2 seconds. Contacts to the n-type material were annealed Ni while annealed Al was used for the contacts to the p-type films.

Table II. Hall mobility measurements of  $\beta$ -SiC films

Sample	Carrier Concentration ( $cm^{-3}$ )	Mobility ( $cm^2/Vs$ )
N1	$1 \times 10^{18}$	226
N2	$2 \times 10^{17}$	420
P1	$2 \times 10^{20}$	16
P2	$3.8 \times 10^{19}$	30
P3	$4 \times 10^{18}$	28

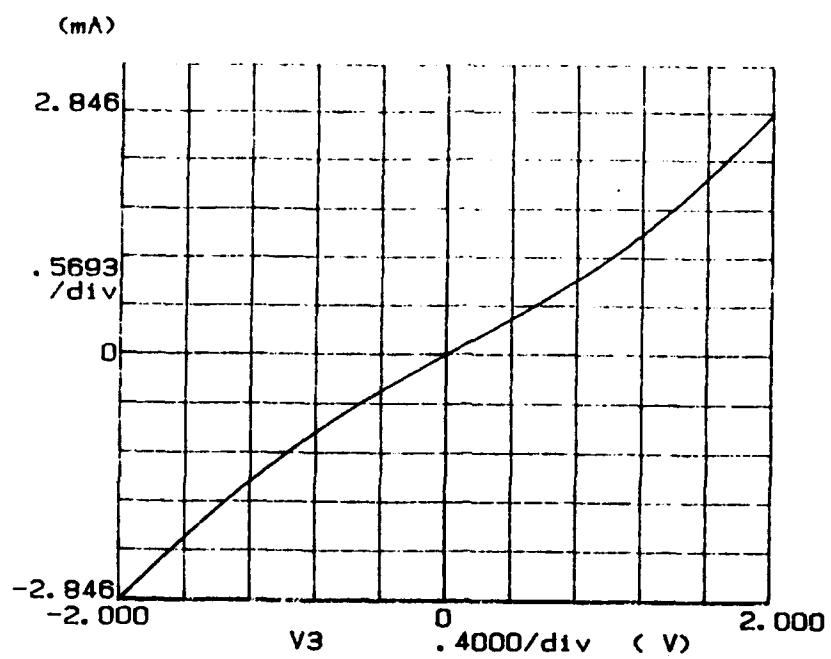


Figure 8. I-V characteristics of unannealed Al contacts.

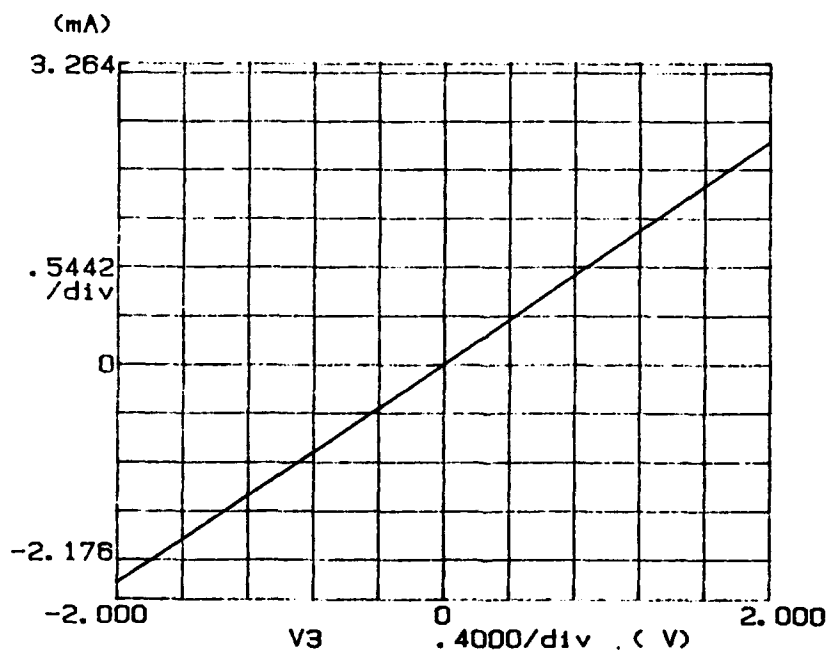


Figure 9. I-V characteristics of annealed Al contacts.

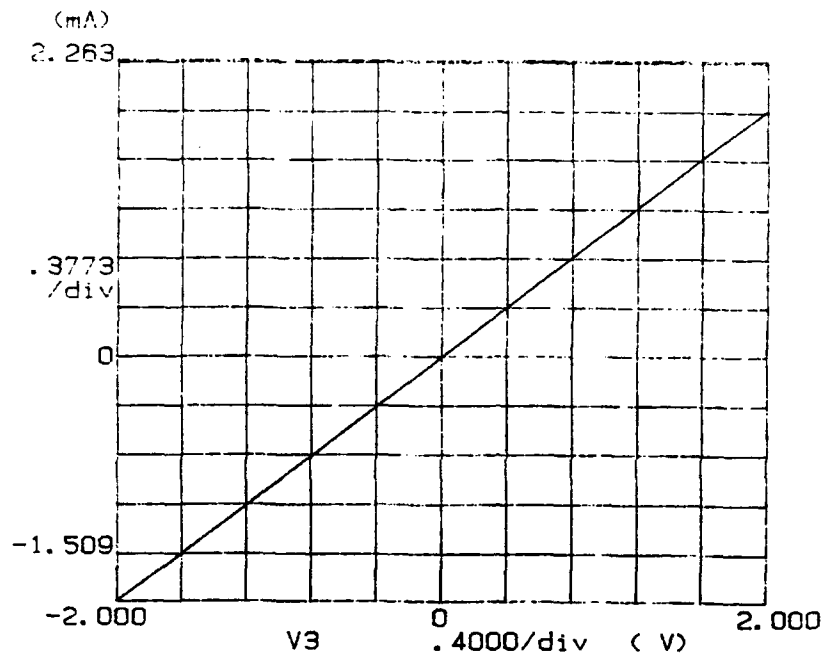


Figure 10. I-V characteristics of annealed Ni contacts.

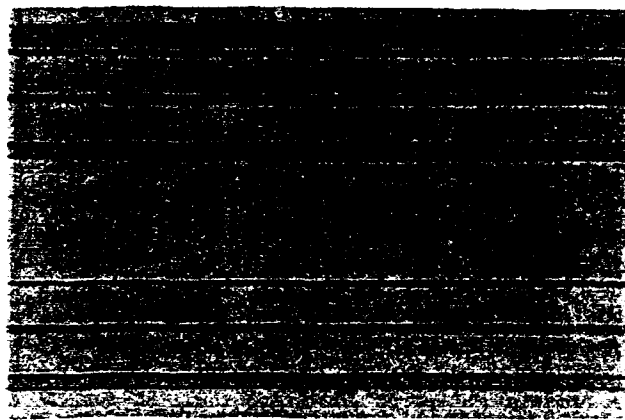
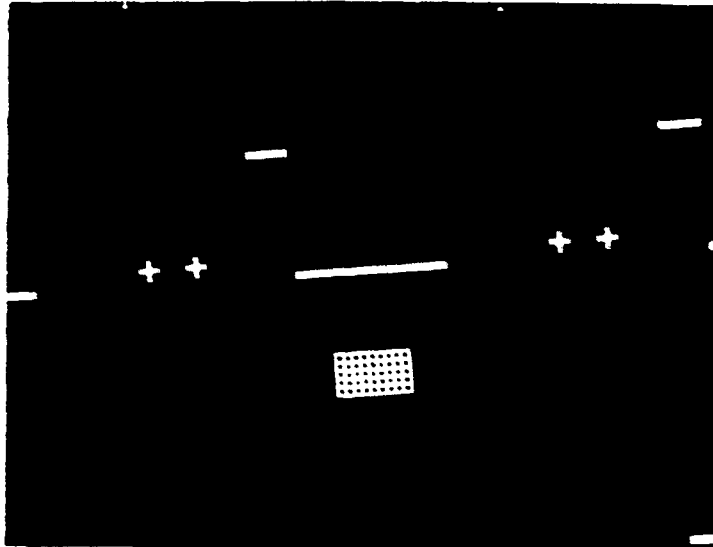
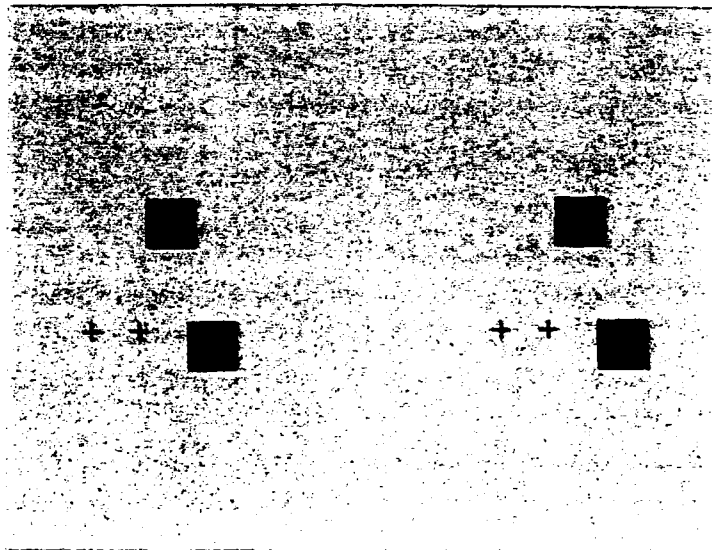


Figure 11. Parallel Ni lines produced by lift-off technique.

*Contact Photolithography Masks.* A six-level mask system has been designed and completed for producing trench HBTs. Optical micrographs of the six masks are presented in Fig. 12. The chip designed contains four transistors: a planar transistor, two trench transistor with trenches of differing length and a "waffle iron" type transistor to maximize the active area/device foot-print. The role of each mask is detailed in Table III. Thus far only the first level has been completed and the wafers have been sent to Virginia Semiconductor for n- and p- type epitaxial Si deposition for the collector and base regions, respectively.

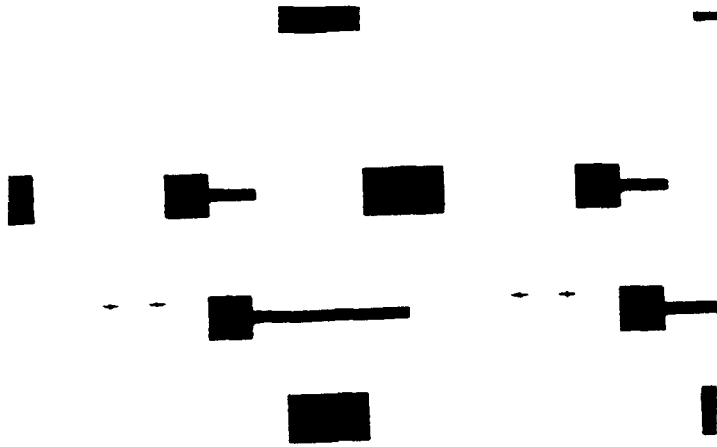


Mask 1: Trench mask

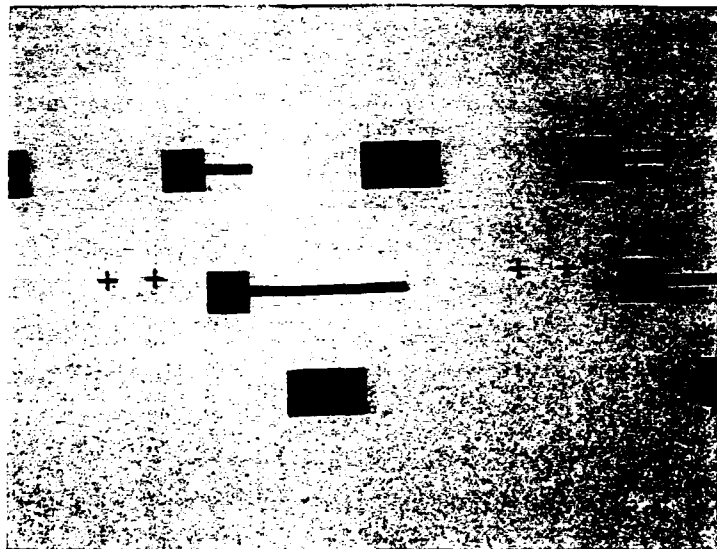


Mask 2: Oxide etch mask.

Figure 12. Masks created for fabricating trench HBTs.

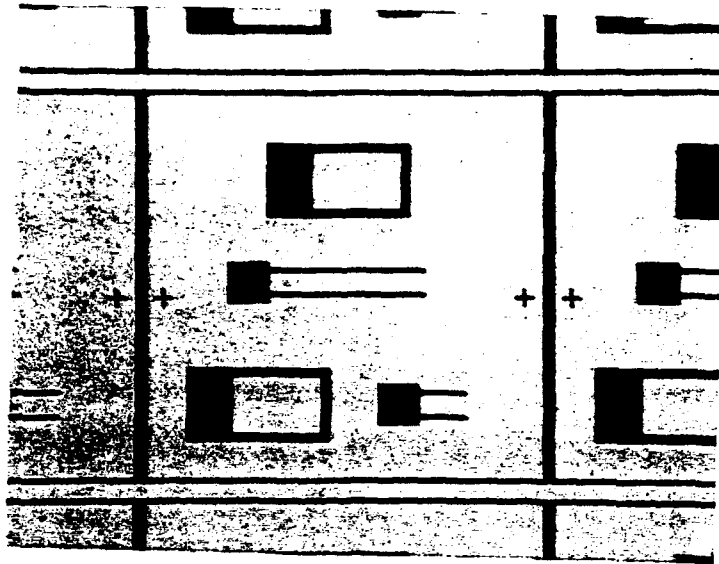


Mask 3: Emitter etch mask.

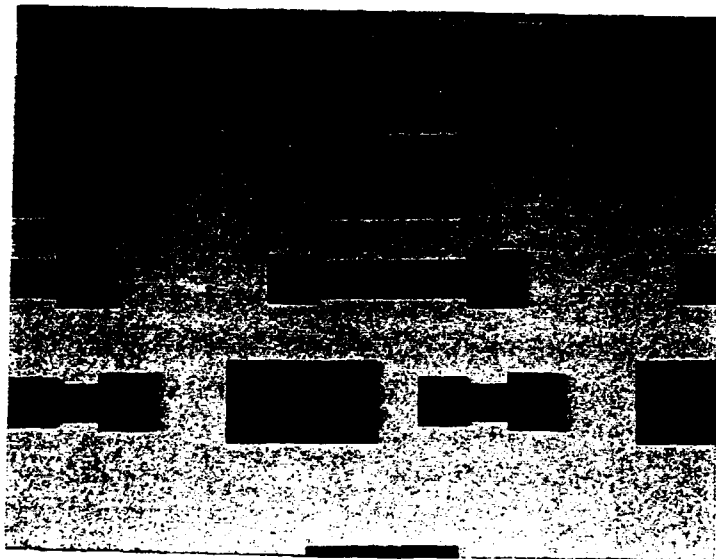


Mask 4: Ni pattern mask.

Figure 12 Con't. Masks created for fabricating trench HBTs.



Mask 5: Al pattern mask.



Mask 6: Isolation mask.

Figure 12 Con't. Masks created for fabricating trench HBTs.

Table III. Role of mask levels in trench HBT fabrication process

<u>Mask Level</u>	<u>Mask Role</u>
1	Pattern oxidized wafer for R.I.E. of trenches
2	Pattern low temperature oxide for electrical isolation of emitter pads
3	Pattern $\beta$ -SiC emitters for R.I.E
4	Pattern Ni contacts
5	Pattern Al contacts
6	Pattern for mesa isolation by Si etch

#### D. Discussion

Continued optimization of deposition parameters has led to separating the deposition of  $\beta$ -SiC on Si(100) substrates into 2 steps. From Figs. 2 and 3 it can be seen that deposition of  $\beta$ -SiC on Si(100) at higher temperatures can lead to substantial pitting. This is attributed to the out diffusion of Si from the substrate through openings in the discontinuous  $\beta$ -SiC film. A "capping"  $\beta$ -SiC layer of  $\approx 100 \text{ \AA}$  has proven to be effective in preventing the out diffusion and therefore the pitting. After the substrate has been "capped," higher temperature growth can be performed. Films deposited at the higher temperatures without using atomic hydrogen exhibit improved crystallinity and the unintentional doping falls by an order of magnitude. This improvement may be due to increased mobility of the surface species leading to fewer electrically active defects in the film.

For device applications, it is necessary to control the carrier concentration of deposited films. Controllable p-type doping across at least three orders of magnitude is possible. N-type doping has not been accomplished directly but rather as a consequence of growth parameters which through optimizing has resulted in unintentional n-type carrier concentrations as low as  $10^{17} \text{ cm}^{-3}$ . Continued work on doping n-type with N from  $\text{NH}_3$  remains to be completed.

Ohmic electrical contacts to both p- and n-type  $\beta$ -SiC have been demonstrated. Although the metal films (Al and Ni) could be deposited and etched after patterning with photoresist, metal etches are not very selective, especially not an etch for Ni. Therefore a lift-off technique is desired where patterning can be achieved with milder solvents. Patterning the Al used as an ohmic contact to p-type  $\beta$ -SiC is easily accomplished by a lift-off technique. However, due to more isotropic coverage, sputtered Ni is difficult to use in a lift-off process, although thin Ni layers can be patterned.

The construction of trenched HBTs is underway. Wafers have been trenched and sent to an outside vendor for Si epitaxial film deposition. Once the wafers are returned, a low temperature

SiO<sub>2</sub> layer will be deposited and patterned (mask 2) for electrical isolation of the emitter contact pads.  $\beta$ -SiC will then be deposited on these substrates and subsequently patterned (mask 3) for the emitters. After this Ni will be sputtered and patterned (mask 4) to make the emitter contacts and then annealed. Al will next be evaporated for the base region contacts, patterned (mask 5) and annealed too. Finally the completed device will be covered with photoresist in a patterning step (mask 6) for mesa isolation.

#### E. Conclusions

1. Optimized processes have been developed for depositing  $\beta$ -SiC on Si(100) and  $\alpha$ -6H-SiC(0001) substrates lowering the unintentional n-type carrier concentration to  $10^{17} \text{ cm}^{-3}$ .
2. Ohmic contacts to n-type  $\beta$ -SiC have been formed with annealed Ni.
3. Ohmic contacts to p-type  $\beta$ -SiC have been formed with annealed Al.
4. Lift-off photolithography process has been applied to patterning sputtered Ni.
5. All photolithography masks have been completed for construction of HBTs.

#### F. Future Research Plans

1. Develop better control over n-type doping.
2. Complete trench heterojunction bipolar transistors using  $\beta$ -SiC emitters.

#### G. References

1. E. O. Johnson, *RCA Rev.* **26**, 163 (1965).
2. R. W. Keyes, *Proc. IEEE* **60**, 225 (1972).
3. *Handbook of Chemistry and Physics*, Editor-in-Chief D. R. Lide, CRC Press, 72<sup>nd</sup> ed., (1991-1992).
4. R. F. Davis, *Physica B* **185**, 1 (1993).
5. R. F. Davis, J. W. Palmour and J. A. Edmond, *Mat. Res. Soc. Symp. Proc.* **162**, 463 (1990).
6. H. P. Liaw and R. F. Davis, *J. Electrochem. Soc.* **131** 3014 (1984).
7. C. C. Chiu and S. B. Desu, *J. Mater. Res.* **8**, 535 (1992).

## IV. Growth of Diamond Particles on a Ni<sub>3</sub>Si Substrate

### A. Introduction

The attainment of heteroepitaxial diamond is important if the microelectronics industry is ever to see the full utility of diamond's unique and excellent properties. Currently, oriented diamond particles have been deposited on c-BN, Si, SiC, Ni and Co. However, there are limitations to these substrate systems. For c-BN, this limitation is the difficulty in obtaining single crystal c-BN substrates of reasonable size. In growth on Si and SiC, there are problems with the large lattice mismatch (around 34% for Si and 18% for SiC) which results in misorientation in the resulting diamond particles. And for Ni and Co, while there is an excellent lattice match, there are adhesion problems and difficulty in obtaining complete films of diamond. A combination of two of the systems in which orientation has already been observed, Ni and Si, has been utilized as a substrate for heteroepitaxial diamond. By forming a nickel silicide, one combines the lattice match of the nickel with silicon's ability for covalent overlap and improved interface chemistry. Also, by introducing Ni into Si, the surface energy should increase from 870 ergs/cm<sup>2</sup> [1] to 1740 ergs/cm<sup>2</sup> [2] at room temperature, which may assist in the two-dimensional nucleation of diamond. Specifically, our primary candidate from the nickel silicide system is Ni<sub>3</sub>Si which is cubic (Cu<sub>3</sub>Au-type structure) and has a small lattice mismatch with diamond (approximately 2%).

### B. Experimental

Currently, a bulk nickel silicide is being utilized. This silicide was produced by an arc melting and drop casting technique and involved mixing stoichiometric amounts of the nickel and silicon components to produce the compound Ni<sub>3</sub>Si. The silicide sample was produced by Dr. C.T. Liu at Oak Ridge National Laboratory in the Metals and Ceramics Division. The resulting silicide was polycrystalline with small grains (average grain size was approximately 20 μm in diameter) and has been characterized by metallography, XRD (both diffractometer and Debye-Scherrer), XPS, AES, and TEM as being largely cubic Ni<sub>3</sub>Si. Diamond films were deposited on these substrates in a hot-filament chemical vapor deposition chamber connected *in-vacuo* with XPS and AES. Also, so that comparisons could be made with the chemistry of the nickel system, the same conditions were utilized in depositing on polycrystalline nickel. Typical conditions were a filament temperature of over 2200°C, substrate temperature of approximately 850 °C, pressure of 20 Torr, and methane concentration of 1% in hydrogen. The resulting films were characterized by SEM, Raman, XPS and AES.

### C. Results and Discussion

An optical micrograph of the silicide sample is presented in Fig. 1 and gives evidence for the existence of two phases. In Fig. 2, the XRD diffractometer pattern of the silicide is plotted. The

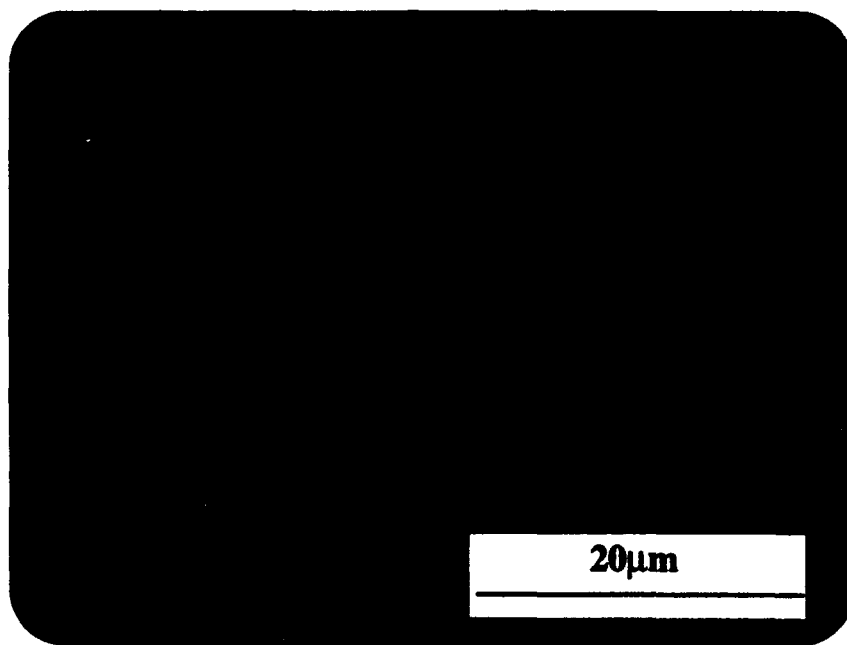


Figure 1. Optical micrograph of bulk nickel silicide sample at 500X.

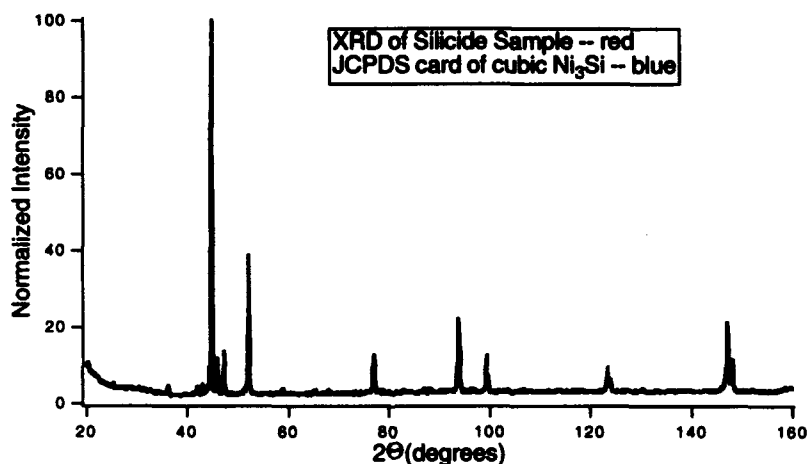


Figure 2. XRD pattern of nickel silicide sample.

peaks match up quite well with the powder pattern for cubic  $\text{Ni}_3\text{Si}$ . However, there are two peaks at a  $2\theta$  of  $46.0^\circ$  and  $47.3^\circ$  that are not accounted for by the cubic pattern. These peaks did correspond to that of the high temperature  $\text{Ni}_3\text{Si}$  phase which is a monoclinic material. In corroboration of the stoichiometry, XPS and AES quantitative analysis gave a  $X_{\text{Ni}}/X_{\text{Si}}$  ratio of approximately 3. Also, TEM showed the presence of two phases: one the cubic  $\text{Ni}_3\text{Si}$  and the second a distorted cubic structure, which was possibly monoclinic.

In Fig. 3, two SEM micrographs resulting from diamond growth on the silicide are presented. There appears to be some evidence for oriented particles on the silicide. Figure 4 shows two SEM micrographs from growth on the nickel. As can be seen, the majority of the growth on the nickel substrate had DLC growth as in the top micrograph of Fig. 4. There also was poorly faceted diamond on the sample, as in the bottom micrograph of Fig. 4. Figures 5 and 6 are the Micro-Raman spectra for diamond growth on the nickel silicide and nickel, respectively. The Raman for growth on the nickel silicide, obviously, shows a very strong diamond peak centered at  $1334\text{ cm}^{-1}$  with a FWHM of  $3.6\text{ cm}^{-1}$  and very little  $sp^2$  component. For growth on the nickel, however, the Raman shows a very weak and broad diamond peak and a large  $sp^2$  peak.

#### D. Conclusions

Diamond particles were obtained on the nickel silicide where, under the same conditions, graphite and DLC was obtained on the pure nickel substrate. There seems to be some evidence that oriented particles were obtained on the nickel silicide. More interesting, however, may be the result that the addition of even a small amount of silicon to the nickel greatly changes the chemical properties from that of pure nickel.

#### E. Future Research

The nucleation density attained was quite small and was on the order of  $10^5$ . This is as would be expected for a material that has not been scratched or biased. We would, however, like to increase this nucleation density by biasing. Also, this proof of concept suggests that if single crystal nickel silicide can be obtained, it may be a heteroepitaxial substrate for diamond. Thus, we will also be working on methods to obtain single crystal nickel silicide, or, at least, a larger grained material.

#### F. Acknowledgments

Dr. C.T. Liu of the Metals and Ceramics Division is gratefully acknowledged for the fabrication of the silicide material used in this research. We appreciate the assistance of Ambika Somashekhar and Dr. Robert Nemanich for their Raman support. Also, we appreciate Dr. Nadia El-Masry's assistance in examining the TEM results.

#### G. References

1. K.-N. Tu, J. W. Mayer, L. C. Feldman, *Electronic Thin Film Science for Electrical Engineers and Materials Scientists* (Macmillan Publishing Company, New York, 1992), p. 38.
2. B. J. Keene, *Surface and Interface Analysis* **10**, 367 (1987).

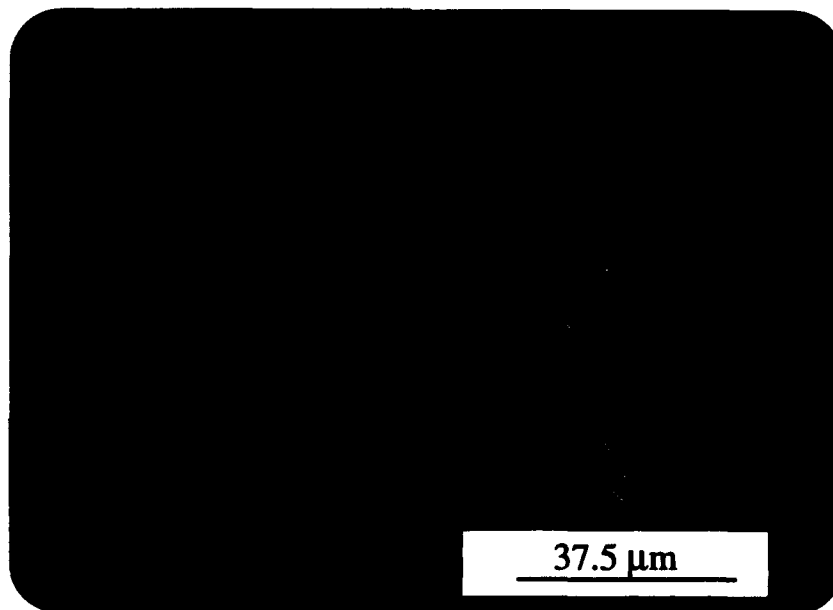
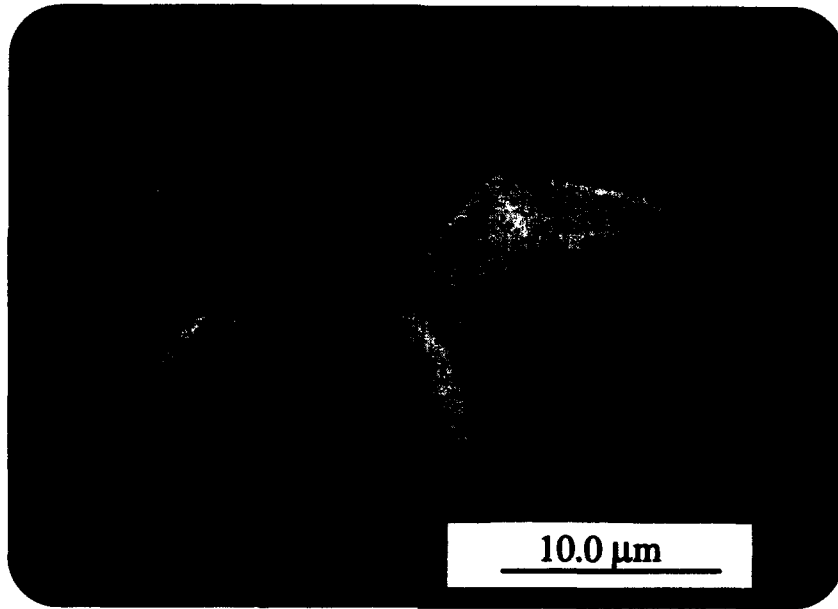


Figure 3. SEM micrographs of diamond particles on the nickel silicide.

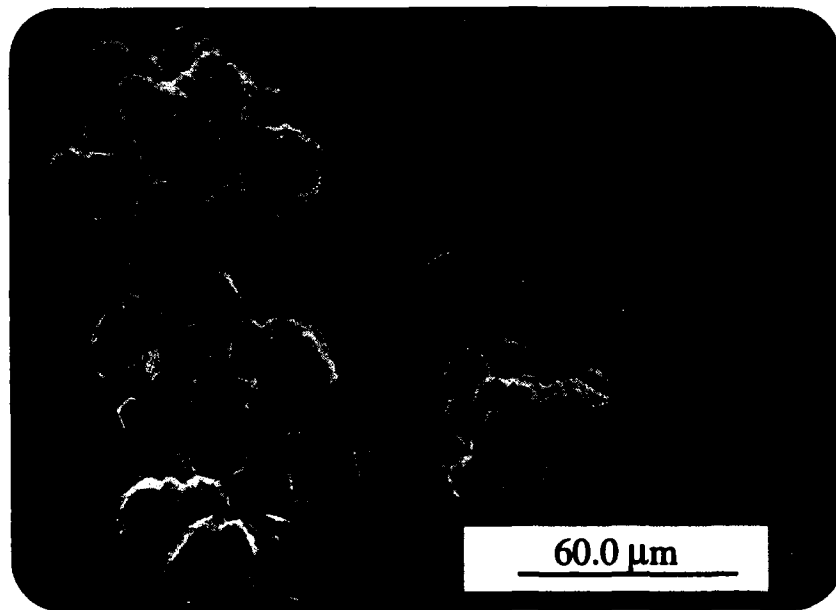
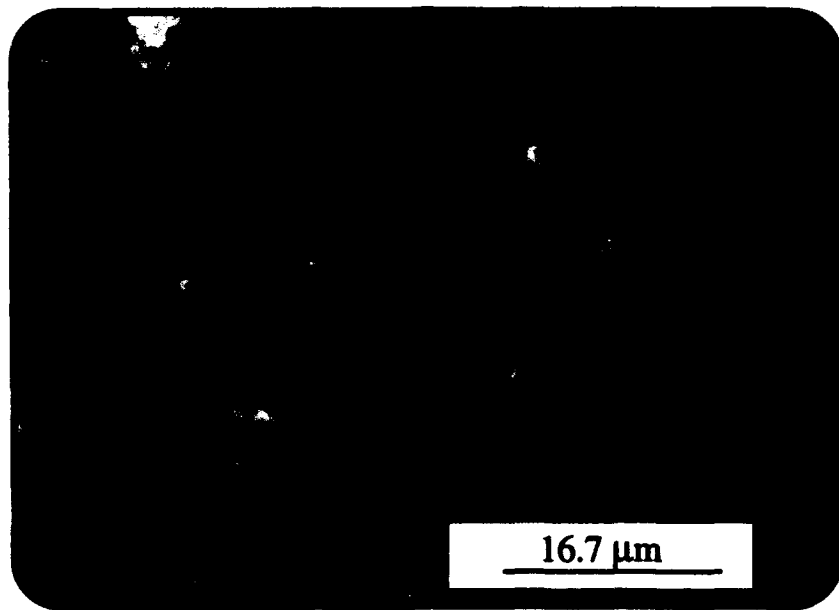


Figure 4. SEM micrographs of growth on the nickel.

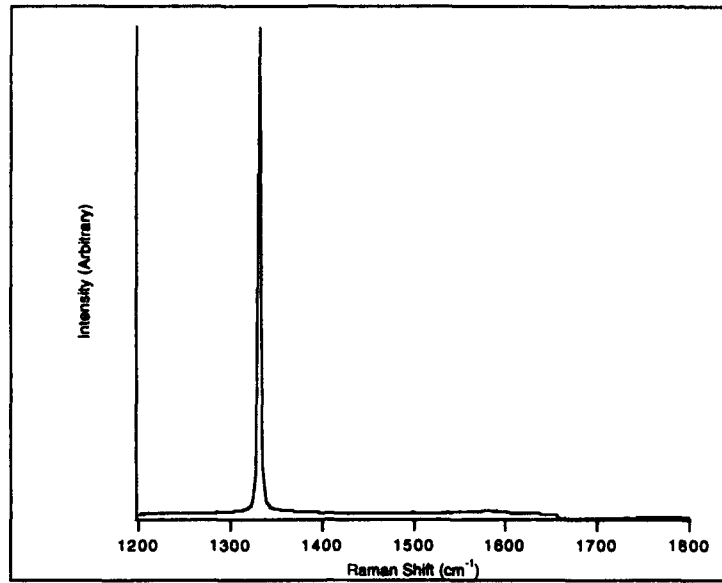


Figure 5. Micro-Raman of growth on the nickel silicide.

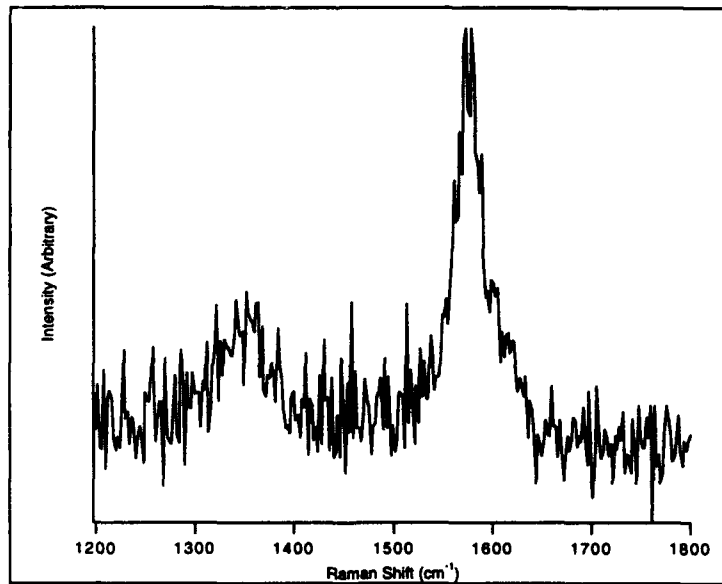


Figure 6. Micro-Raman of growth on the nickel.

## V. Electrical Characterization of Epitaxial CeO<sub>2</sub> on Si (111)

### A. Introduction

Cerium oxide (CeO<sub>2</sub>) is interesting because it has a cubic structure which is nearly lattice matched to silicon and a high dielectric constant ( $\approx 26$ ). The lattice mismatch  $\Delta a/a$  for CeO<sub>2</sub> to Si is 0.35%. This value is better than the respective values for other crystalline insulators such as CaF<sub>2</sub>, yttria-stabilized cubic zirconia, sapphire, and spinel. A potential application for CeO<sub>2</sub> is as the insulating layer in a silicon-on-insulator (SOI) structure. This epitaxial ceramic would have advantages over another SOI technique called separation by implanted oxygen (SIMOX), because it would be easy to know and control the thickness of both the ceramic and the Si layers, while potentially lowering the defect density in the latter. CeO<sub>2</sub> can offer an alternative to the previously investigated CaF<sub>2</sub> epitaxial oxides, yielding better properties due to the close lattice match with Si and the greater stability of the CeO<sub>2</sub> films.

It has been shown that crystalline layers of CeO<sub>2</sub> may be grown on a Si substrate both by electron-beam evaporation[1,2] and by laser ablation[3-6]. Favorable growth conditions have been reported[5], and models for the growth modes of CeO<sub>2</sub> on Si have been suggested[7-9]. However, the electrical properties were not reported. We report here the electrical properties of CeO<sub>2</sub> films, as determined from capacitance-voltage and current-voltage measurements, and how modifying the CeO<sub>2</sub>/Si interface can improve these properties.

### B. Experimental Procedure

Silicon (111) wafers (p-type : 0.5  $\Omega$ -cm) 5 cm in diameter were cleaned according to the following procedure. After degreasing, they were soaked in a hot solution of HCl:H<sub>2</sub>O<sub>2</sub>:H<sub>2</sub>O, followed by a dip in dilute HF and a rinse in deionized water. Next the wafers were submerged in a hot solution of NH<sub>3</sub>OH:H<sub>2</sub>O<sub>2</sub>:H<sub>2</sub>O, dipped in dilute HF, and loaded directly into the vacuum system. The substrates were heated under vacuum at  $\approx 800^\circ\text{C}$  until a streaky RHEED pattern was observed ( $\approx 20$  min.). Epitaxial CeO<sub>2</sub> films were grown by irradiating a commercially obtained CeO<sub>2</sub> (99.9%) target with a 193nm wavelength beam from an excimer laser using ArF. The beam was directed into the growth chamber by an optical delivery system consisting of 3 mirrors and a lens, and introduced through a fused silica window. Power of the beam incident on the target was controlled by varying the position of the focussing lens. The energy density for a typical experiment is estimated to be 10 J/cm<sup>2</sup> during each laser pulse. The substrate was maintained at 750°C by means of a quartz lamp heater. During growth, both the substrate and the target were continuously rotated for better film uniformity. The distance between the target and the substrate was varied between 2 and 7 cm. Base pressure in the growth chamber was  $1 \times 10^{-9}$  torr or better and was achieved using a 400 l/s ion pump. Pressure during growth typically rose as high as  $5 \times 10^{-8}$  torr, due to outgassing of heated components.

After growth, some of the films were subjected to an *ex situ* dry O<sub>2</sub> anneal in a furnace at 900°C for varying lengths of time. Films were investigated by ellipsometry and HRTEM. MOS capacitors were constructed on the films by evaporating 0.2 μm thick aluminum dots, 20 mils in diameter, onto the CeO<sub>2</sub> surface, and uniform Al onto the back of the Si (111) wafer.

### C. Results and Discussion

Investigation by *in situ* RHEED indicates that the surface of the ablated films consisted of good quality single-crystal CeO<sub>2</sub> with the (111) orientation. Figure 1A shows a HRTEM micrograph of CeO<sub>2</sub> as deposited on Si(111) substrate. The CeO<sub>2</sub> overlayer is seen to be single crystal with B-type orientation to the Si(111) substrate, and contains several line defects. At the interface two distinct amorphous regions can be seen. The bright contrast layer next to the substrate is SiO<sub>2</sub>, and the dark contrast layer above that is believed to be oxygen deficient α-CeO<sub>x</sub>. We have already presented a model identifying and explaining the existence of these amorphous layers[7,8]. Figures 1B and 1C show HRTEM micrographs of the same CeO<sub>2</sub> film after annealing in a dry O<sub>2</sub> atmosphere at 900°C for 18 and 35 minutes respectively. In these figures it is clear that the α-CeO<sub>x</sub> layer has been removed and the SiO<sub>2</sub> layer has increased in thickness, leaving a CeO<sub>2</sub>/SiO<sub>2</sub>/Si structure. The 18 and 35 minute anneals in oxygen increased the SiO<sub>2</sub> layer to 70Å and 190Å thick respectively, from the as-grown value of 26Å. Ellipsometry measurements agree closely with HRTEM measurements of film thicknesses, and indicate that the deposited films have refractive indexes between 2.2 and 2.4, for 632.8nm wavelength.

Altering the structure of the film from CeO<sub>2</sub>/α-CeO<sub>x</sub>/SiO<sub>2</sub>/Si(111) to CeO<sub>2</sub>/(thicker) SiO<sub>2</sub>/Si(111) greatly enhanced the electrical properties of the films. This is readily seen in Fig. 2, which shows high-frequency (100kHz) capacitance-voltage curves measured on MOS capacitors constructed directly on the films shown in Fig. 1. The as-grown film exhibits fairly high capacitance at accumulation as expected, due to the high dielectric constant. However, the as-grown film is observed to have a low breakdown voltage and to go into deep-depletion as opposed to inversion. The capacitance at accumulation for the annealed films is reduced due to the thicker SiO<sub>2</sub> layers, yet both annealed films show marked improvement in all other aspects of C-V behavior. For instance, inversion is achieved for the annealed films. The hysteresis observed in the C-V curves in Fig. 2 was detected by sweeping the voltage from inversion to accumulation and back again. This hysteresis may be caused by trapped charge. The large amount of hysteresis in the C-V curve of the as-grown film indicates a significant amount of trapped charge, while the C-V curve for the 35 minute annealed sample has negligible hysteresis, which is comparable to thermally grown SiO<sub>2</sub>.

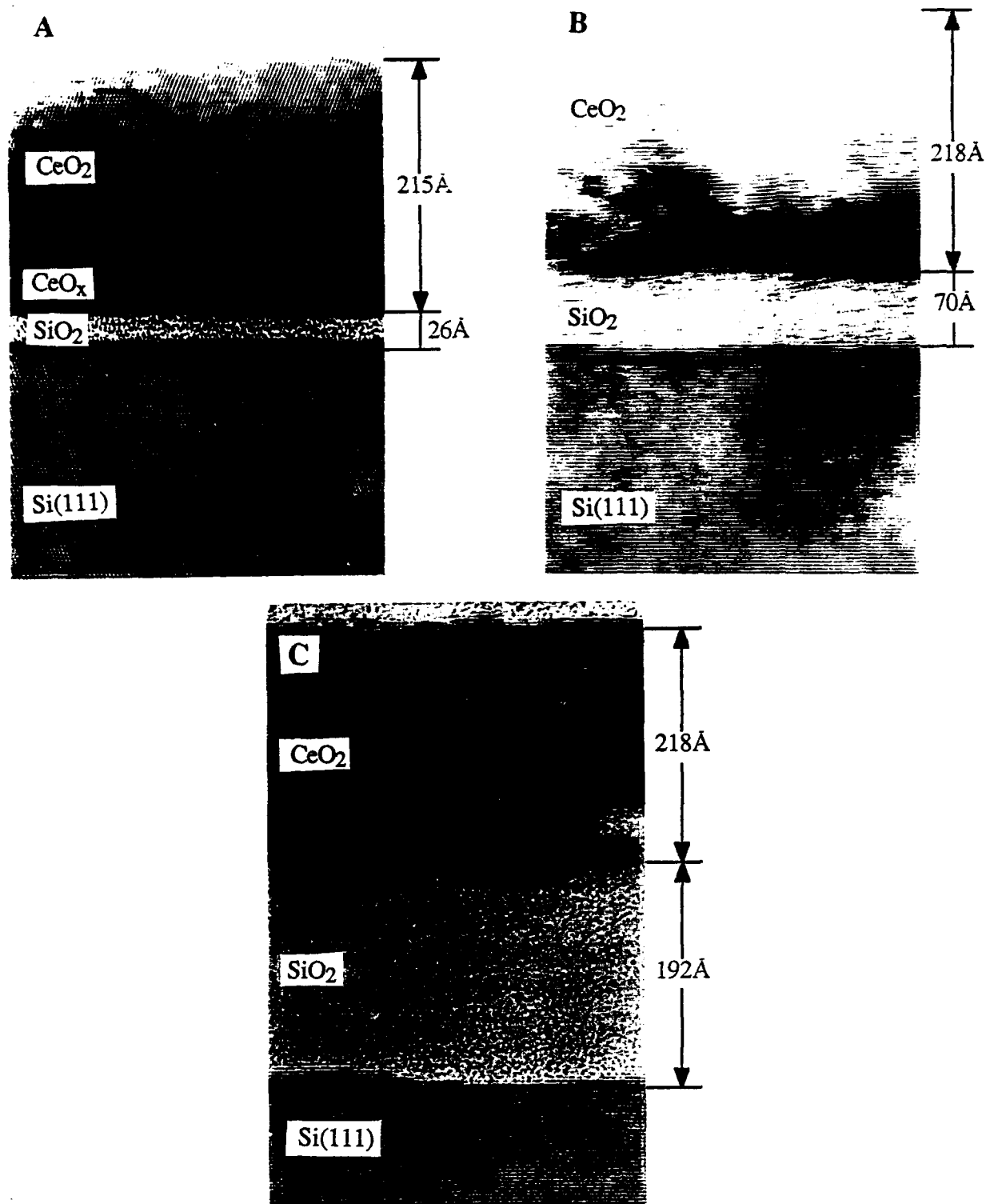


Figure 1. Cross-sectional HRTEM view of (A) CeO<sub>2</sub> on Si(111) as deposited, (B) after 18 minutes annealing at 900°C in dry O<sub>2</sub>, and (C) after 35 minutes annealing at 900°C in dry O<sub>2</sub>.

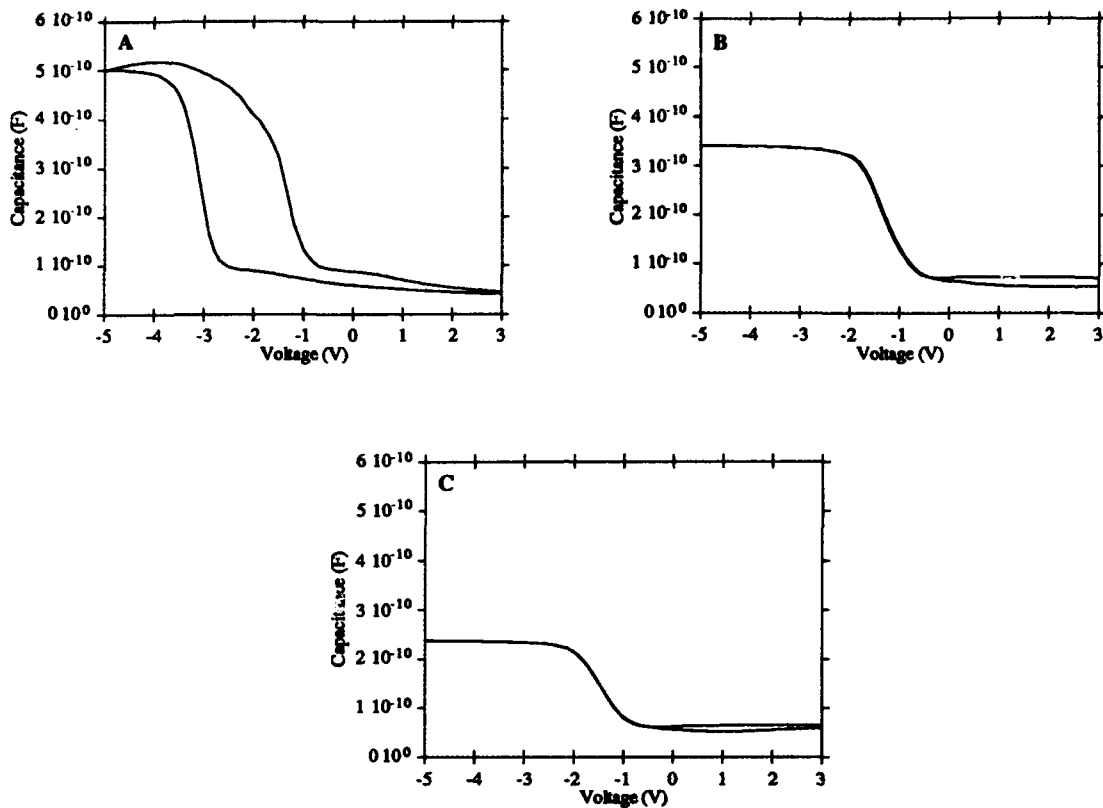


Figure 2. High frequency (100kHz) capacitance vs. voltage curves, swept from inversion to accumulation and back, for (A)  $\text{CeO}_2$  on Si(111) as deposited, (B) after 18 minutes annealing, and (C) after 35 minutes annealing. Dots are 20 mil diameter Al.

These measured C-V curves were compared to theoretical C-V curves in order to calculate the fixed oxide charge density  $Q_f$ , and all results are summarized in Table I. Annealing is seen to slightly lower  $Q_f$  to  $5 \times 10^{11} \text{ cm}^{-2}$ . Thermal oxides on Si(111) would typically be annealed in a forming gas to lower  $Q_f$  to  $\sim 1 \times 10^{11} \text{ cm}^{-2}$ . The density of interface traps  $D_{it}$  was also lowered by annealing to  $6 \times 10^{11} \text{ cm}^{-2}$ , which is comparable to a thermal oxide on a Si(111) surface, for example  $D_{it} = 5 \times 10^{11} \text{ cm}^{-2}$  [11]. The annealed structure has the benefits of a good  $\text{SiO}_2/\text{Si}$  interface, which is electrically favorable.

The high-frequency capacitance of the  $\text{CeO}_2$  films at accumulation varied with the frequency of the AC signal. By changing the measuring frequency from 100kHz to 20Hz,  $C_{ox}$  (18 minute anneal) was changed from 360pF to 570pF, and  $C_{ox}$  (35 minute anneal) was changed from 230pF to 290pF. Quasi-static C-V responses were obtained for the annealed films, but typically  $C_{ox}(\text{quasi-static})$  were a factor of 2 times higher than  $C_{ox}(100\text{kHz})$ , and they could not be compared to the high-frequency C-V curves. Because the series resistance

was low ( $< 50\Omega$ ) for these samples, this behavior is believed to be caused by dipoles in the deposited films. However, it is unclear at this stage whether dipoles exist in the  $\text{CeO}_2$  or are the result of impurities contained in the films, as the  $\text{CeO}_2$  target was commercially obtained and 99.9% pure. In effect, the relative dielectric constant  $\epsilon_r$  of our  $\text{CeO}_2$  films depends on the frequency of measurement. For quasi-static measurements, the value for  $\epsilon_r$  of  $\sim 26$  was confirmed.

Table I. Comparison of electrical properties of as-grown  $\text{CeO}_2$  on Si(111), oxygen annealed  $\text{CeO}_2$  on Si(111), and thermally grown  $\text{SiO}_2$  on Si(111) determined from C-V measurements.

	As-Grown	18 min Oxidation	35 min. Oxidation	Thermal $\text{SiO}_2$ on Si (111)
$\text{CeO}_2$ thickness ( $\text{\AA}$ )	215	218	213	-
$\text{SiO}_2$ thickness ( $\text{\AA}$ )	26	70	192	-
fixed oxide charge density $Q_f$ ( $\text{cm}^{-2}$ )	$7 \times 10^{11}$	$5 \times 10^{11}$	$5 \times 10^{11}$	$1 \times 10^{11}$
oxide trapped charge density $Q_{ot}$ ( $\text{cm}^{-2}$ )	$\sim 10^{12}$	$\sim 10^{10}$	-	-
interface trap density $D_{it}$ ( $\text{cm}^{-2}$ )	$2 \times 10^{12}$	$7 \times 10^{11}$	$6 \times 10^{11}$	$5 \times 10^{11}$

The breakdown strength of the  $\text{CeO}_2$  films was also improved by oxygen annealing. This is clearly seen in Fig. 3, which shows the current-voltage (I-V) response of the as-grown and annealed films at accumulation. The as-grown film is stable up to an applied voltage of about 5V, which, neglecting the very thin  $\text{SiO}_2$  layer, corresponds to an electric field of  $\sim 2.5$  MV/cm. Above 5V, the as-grown film exhibits self-healing breakdown. The annealed films have recognizable I-V responses, with increasing breakdown strength as the  $\text{SiO}_2$  layer thickens and the quality of  $\text{CeO}_2$  is improved. It is possible to estimate the electric fields in both the  $\text{CeO}_2$  and  $\text{SiO}_2$  layers by assuming the dielectric constants to be 26 and 3.9 respectively, and assuming there is no high density of trapped charge at the  $\text{CeO}_2/\text{SiO}_2$  interface. For example, in Figure 3B for the 18 minute annealed sample, it can be shown that for an applied voltage of 8V, the fields in  $\text{SiO}_2$  (70 $\text{\AA}$ ) and  $\text{CeO}_2$  (218 $\text{\AA}$ ) are  $\sim 8$  MV/cm and  $\sim 1.5$  MV/cm respectively. The gradual increase in current for applied voltage larger than 8 can be due to field assisted tunnelling in  $\text{SiO}_2$ . Further increasing the applied voltage beyond  $\sim 12$ V yields electric fields in excess of 10MV/cm in the

SiO<sub>2</sub>, which results in the breakdown of this layer. Comparable conclusions can also be reached from the data in Figure 3C. We expect that the breakdown field of the annealed CeO<sub>2</sub> is better than 2.5MV/cm.

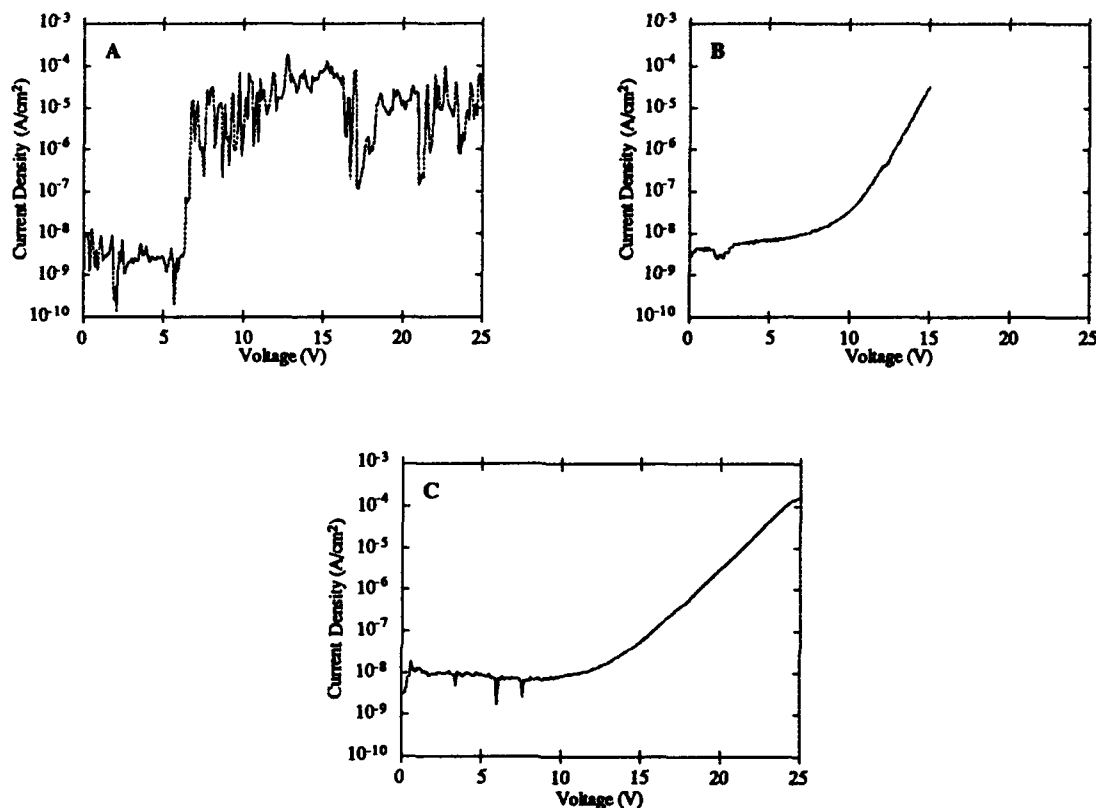


Figure 3. Current vs. voltage curves, measured in accumulation for (A) CeO<sub>2</sub> on Si(111) as deposited, (B) after 18 minutes annealing, and (C) after 35 minutes annealing. Dots are 20 mil diameter Al.

#### D. Conclusions

To summarize, electrical properties of epitaxial CeO<sub>2</sub> on Si(111) substrates were investigated through capacitance-voltage and current-voltage measurements. Although as-deposited CeO<sub>2</sub> films exhibit high capacitance at accumulation, they break down at low field strengths and go in to deep-depletion. The C-V performance of these films was greatly improved by annealing in an oxygen atmosphere, leading to a CeO<sub>2</sub>/SiO<sub>2</sub>/Si structure. After annealing, the breakdown field was increased and inversion was achieved. The fixed oxide charge and the interface trap density were reduced by annealing. This may be a result of utilizing the electrically excellent SiO<sub>2</sub>/Si interface, followed by the single crystal CeO<sub>2</sub> dielectric film lattice matched to silicon. This CeO<sub>2</sub>/SiO<sub>2</sub>/Si structure is shown to be a legitimate

candidate for SOI device applications, especially if such performance can still be achieved for growth on the Si(100) surface. Also, the quality of Si on CeO<sub>2</sub> is not yet investigated. However, the current result shows an initial and encouraging step towards a new lattice matched SOI structure.

#### E. Plans for Future Research

As mentioned, the growth of CeO<sub>2</sub> on Si(100) substrates is desirable. Perhaps 3° or 4° off-axis substrates would allow the crystalline growth of CeO<sub>2</sub> (100). Low temperature growth should be attempted in order to control the reaction that takes place at the interface. It may be possible to eliminate this reaction completely, although we have shown that the SiO<sub>2</sub> layer at the interface may be beneficial to the electrical properties. Also, the quality of Si grown on CeO<sub>2</sub> should be investigated.

#### F. References

1. T. Inoue, Y. Yamamoto, S. Koyama, S. Suzuki, and Y. Ueda, *Appl. Phys. Lett.*, **56**, 1332 (1990).
2. T. Inoue, T. Oshuna, L. Luo, X. Wu, C. Maggiore, Y. Yamamoto, Y. Sakurai, and J. Chang, *Appl. Phys. Lett.*, **59**, 3604 (1991).
3. H. Koinuma, H. Nagata, T. Tsukshara, S. Gonda, and M. Yoshimoto, *Extended Abstracts of the 22nd Conference on Solid State Devices and Materials, Sendai, Japan, 1990* p. 933.
4. L. Tye, Y. He, R. Leonard, N. El-Masry, and S. M. Bedair, presented at the 35<sup>th</sup> Electronic Materials Conference, Santa Barbara, CA, 1993.
5. H. Koinuma, H. Nagata, T. Tsukshara, S. Gonda, and M. Yoshimoto, *Appl. Phys. Lett.*, **58**, 2027 (1991).
6. H. Nagata, T. Tsukshara, S. Gonda, M. Yoshimoto, and H. Koinuma, *Jpn. J. Appl. Phys.*, **30**, L1136 (1991).
7. T. Chikyow, L. Tye, N. A. El-Masry, and S. M. Bedair, *App. Phys. Lett.* (submitted).
8. T. Chikyow, L. Tye, N. A. El-Masry, and S. M. Bedair, presented at the Materials Research Society Fall Meeting, Boston, MA, 1993.
9. M. Yoshimoto, H. Nagata, T. Tsukshara, and H. Koinuma, *Jpn. J. Appl. Phys.*, **29**, L1199 (1990).
10. S. Wainwright and S. Hall, *Semicond. Sci. Technol.*, **8**, 1854, (1993).
11. E. Nicollian and J. Brews, *MOS Physics and Technology*, John Wiley and Sons, New York, (1982).

## VI. Distribution List

Mr. Max Yoder Office of Naval Research Electronics Division, Code: 1114SS 800 N. Quincy Street Arlington, VA 22217-5000	3
Administrative Contracting Officer Office Of Naval Research Resident Representative The Ohio State University Research Center 1960 Kenny Road Columbus, OH 43210-1063	1
Director, Naval Research Laboratory ATTN: Code 2627 Washington, DC 20375	1
Defense Technical Information Center Bldg. 5, Cameron Station Alexandria, VA 22314	12